FAST: A Future Aircraft Sizing Tool for Conventional and Electrified Aircraft Design

Paul R. Mokotoff*, Maxfield Arnson*, Yi-Chih Wang*and Gokcin Cinar†
Department of Aerospace Engineering, University of Michigan, Ann Arbor, Michigan 48109

Electrified aircraft are a promising solution to reduce aviation's carbon footprint across general and commercial aviation sectors. However, many current conceptual design studies assume fixed propulsion architectures and operations, limiting design flexibility and potentially leading to sub-optimal outcomes. To address this, the Future Aircraft Sizing Tool (FAST), an open-source, Matlab-based tool, was developed as a propulsion system-agnostic tool for early-phase conceptual design. FAST facilitates rapid and comprehensive aircraft sizing and performance evaluation, utilizing an extensive database of over 450 historical aircraft. It combines data-driven models with physics-based models where historical data is insufficient, particularly for new electrification technologies. This capability enables early-stage design space exploration to rigorously assess a wide range of propulsion architectures, energy sources, and operational strategies for novel aircraft configurations. This paper presents the key features of FAST, including workflows for aircraft sizing and analysis. The paper also presents a case study involving a commercial freighter, demonstrating FAST's ability to perform design space exploration and early-phase trade studies.

Nomenclature

DSM	=	Design Structure Matrix
EAP	=	Electrified Aircraft Propulsion
EIS	=	Entry-into-Service
EPFD	=	Electrified Powertrain Flight Demonstration
FAA	=	Federal Aviation Administration
FAST	=	Future Aircraft Sizing Tool
GPM	=	Gaussian Process Model
ICAO	=	International Civil Aviation Organization
MTOW	=	Maximum Takeoff Weight
OEW	=	Operational Empty Weight
SLS	=	Sea-Level Static
SUSAN	=	Subsonic Single Aft Engine
TCDS	=	Type Certificate Data Sheets
TLAR	=	Top Level Aircraft Requirements
TOGW	=	Takeoff Gross Weight

I. Introduction

Over the last decade, electrified aircraft design has gained significant attention as a promising technology to curb aviation's harmful CO_2 emission contributions. Electrified aircraft, which is a general term used for fully electric, hybrid electric, and turboelectric configurations, incorporate electrical components in the powertrain, such as electric motors, generators, power converters, or batteries, to name a few. The primary system-level benefits associated with aircraft electrification include: reduced CO_2 emissions during operation due to decreased fuel burn; and reduced thermal and acoustic signatures (less heat and noise released from its operation). These benefits come from decoupling

*Graduate Research Assistant, Department of Aerospace Engineering, University of Michigan, Ann Arbor, Michigan 48109, AIAA Student Member.
†Assistant Professor, Department of Aerospace Engineering, University of Michigan, Ann Arbor, Michigan 48109, AIAA Senior Member.

the gas-turbine engine and propulsor, allowing them to operate at their own optimal speeds [1]. Significant funding and efforts have been invested into electrified aircraft design, especially for the Electrified Aircraft Propulsion (EAP) program at NASA [2] and their Electrified Powertrain Flight Demonstration (EPFD) Project [3]. These programs help make flight more sustainable by testing new electrified aircraft propulsion technologies and understanding the difficulties associated with electrifying future aircraft concepts [3]. Thanks to the investments in these programs, many novel conceptual aircraft designs have been developed, such as NASA's Subsonic Single Aft Engine (SUSAN) [4] and Single-Aisle Turboelectric Aircraft with Aft Boundary Layer Propulsion [5] concepts.

Due to an increased interest in electrified aircraft design, recent literature has focused on analyzing electrified aircraft performance as well as exploring the electrified aircraft design space for different configurations and operational modes. Cinar et al. [6] modeled a ATR 42-600, but re-designed it with a parallel hybrid-electric propulsion architecture. One of the four different operational modes explored by Cinar et al. included peak power shaving, in which power from an electric motor supplements the takeoff/climb power provided by the aircraft's gas-turbine engines. By using 50 to 100% of the electric motor's power available and turning off the electric motor between 12,000 and 24,000 ft, between 709 and 715 kg of fuel was burned for a 500 nmi mission [6]. This work established a foundation for a larger design space exploration and sensitivity study [7], in which they varied the electric components' technology levels and operational strategies for the parallel hybrid-electric aircraft. They found that electrifying ground taxi (spinning the propellers with electric motors instead of gas-turbine engines) yielded significant fuel savings because the gas-turbine engines were not operating inefficiently on the ground before takeoff. In contrast, re-charging the battery during flight limited the benefits of flying with an electrified aircraft propulsion system. In these studies by Cinar et al, the peak power shaving strategy involved the electric motor supplementing the gas-turbine engine power. This allows the gas-turbine engines to be downsized and operate more efficiently during cruise, and was demonstrated by Lents et al. [8]. In their work, Lents showed that peak power shaving had the opportunity to save about 5% fuel on a 900 nmi mission for Boeing's Refined SUGAR aircraft. Most of this fuel burn savings was attributed to optimizing the downsized engine for cruise thrust conditions, which reduced the thrust-specific fuel consumption by 2.3%.

Another commonly analyzed configuration is NASA's SUSAN, which is designed to carry 180 passengers for 2,500 nmi [4]. Chau and Kenway [9] explored different propulsion architecture configurations for the SUSAN aircraft. These included ducted turbofans or open rotor tailcone thrusters on the aircraft's tail and counter-rotating propfans or distributed electric propulsion on the wings. The configuration that saved the most fuel included an aft ducted turbofan and 16 electric motors distributed on the wings, which burned 26.8% less fuel than a Boeing 737-800 (with 2005 technology levels) on a 750 nmi mission. In a later study, Chau and Duensing [10] performed a weight sensitivity study on SUSAN by employing multi-disciplinary design optimization to minimize the aircraft's block fuel on a 2,500 nmi mission. The optimized design included electrified aircraft technologies, but increased the propulsion system's weight by about 27,000 lbm. Despite the weight penalty, the optimized SUSAN configuration burned 8.4% and 9.6% less fuel on 750 and 1,000 nmi missions, respectively, relative to a Boeing 737-800 sized for the same design range and assuming 2020 technology levels. If the Boeing 737-800 was sized for its typical 3,100 nmi design range, then the SUSAN configuration burned 11.1% and 12.5% less fuel on the 750 and 1,000 nmi missions, respectively. Aside from system-level trade studies, Haglage et al. [11] explored a variety of electric bus architectures to transmit power from SUSAN's aft engine to the electric motors on the wing. A direct bus architecture was selected using 16 buses (one for each electric motor), which allowed the electric motors' size to marginally increase in the event that another electric motor failed.

In addition to SUSAN, other regional and advanced single aisle aircraft have been recently studied. These studies only consider a conventional propulsion system with gas-turbine engines, and represent literature focused on making incremental technology improvements to reduce aviation's CO_2 emissions. Cai et al. [12] developed models of a 19-passenger aircraft representative of a Beechcraft 1900D and a 50-passenger aircraft representative of an ATR 42-600. These aircraft models were infused with state-of-the-art technologies expected to be fully developed by 2030, and burned 30.6% and 35.1% less fuel than the conventional 19-passenger and 50-passenger aircraft, respectively. As for single aisle aircraft, Recine et al. [13] developed an advanced Boeing 737 MAX 8 model with state-of-the-art technologies that are expected to be fully developed and flying by 2035. With the integrated advanced technologies, the advanced aircraft burned 18.22% less fuel than the current Boeing 737 MAX 8. In a similar study, Harish et al. [14] developed an advanced A320neo model with state-of-the-art technologies for a 2030 entry-into-service (EIS) year such as advanced nacelle technologies and composite structures on the wing and tail. Using these technologies, approximately 20.45% less fuel was burned than the current A320neo aircraft on the market. Then, Milios et al. [15] used the advanced A320neo model and electrified it with a parallel hybrid-electric propulsion architecture. They also explored multiple operational strategies like Cinar et al. [6] and found that the TSFC at the engine's design point can be reduced by 1.3% to 1.4%.

The literature pertaining to advanced conventional and electrified aircraft design tailors its studies towards one specific propulsion architecture rather than exploring a variety of propulsion architectures. In nearly all of the studies reviewed, it was implicitly assumed that early-phase conceptual design was completed, parts of the aircraft's system architecture were already selected (like the propulsion system), and more detailed analyses (such as preliminary multi-disciplinary design optimization) were being performed for late-phase conceptual design studies. With many novel aircraft configurations and propulsion architectures being developed, there is a need for a conceptual aircraft design and analysis tool that can rapidly generate aircraft designs and allow for early-phase design space exploration while exploring different operational strategies for electrified aircraft concepts. That way, the designer can explore a myriad of electrified aircraft concepts before making design decisions about the propulsion architecture and operational strategies that should be integrated into an aircraft's design.

In collaboration with NASA's EPFD and hybrid-electric research teams, a need for an aircraft sizing tool that can assess the potential performance of a variety of EAP vehicles, predict the sensitivities of a design with respect to major aircraft performance and design parameters, and project future aircraft performance parameters and electrification technology capabilities was identified. One of NASA's primary research goals is to advance aerospace technologies to revolutionize the energy efficiency and environmental compatibility of fixed-wing transport aircraft, regardless of the propulsion architecture. These transport aircraft can be as small as turboprops carrying fewer than 19 passengers (Federal Aviation Administration [FAA] Part 121 aircraft), or larger turboprops to turbofan aircraft carrying between 20 and 300 or more passengers (FAA Part 135 aircraft). Designing aircraft to achieve these goals requires system-level analyses to assess the interdependencies between technologies, as well as possible benefits and drawbacks. Based on NASA's needs and the literature review, a conceptual aircraft sizing tool must be developed to allow for rapid early-phase conceptual design, projecting existing technologies into the future, and facilitating design space exploration studies. Additionally, the tool must enable high-level aircraft optimization for a given set of parametric mission requirements as well as aircraft-level and component-level performance parameters.

The **F**uture **A**ircraft **S**izing **T**ool, **FAST**[*], is an open-source, Matlab-based aircraft sizing tool that fills this void and serves as an early-phase conceptual design tool used to size an aircraft with *any* propulsion architecture. The key distinguishing features within FAST are:

- A rapid aircraft sizing environment to facilitate design space exploration and sensitivity studies for conventional and electrified aircraft (with the ability to add other component-level models for concepts involving hydrogen or other novel fuels), with designs usually converging in less than one-minute
- A database of over 450 conventional, kerosene-powered aircraft to drive regressions for predicting unknown aircraft performance parameters and propulsion system sizing estimates [16]
- An energy-based mission analysis, which requires no assumptions about the aircraft's propulsion architecture, thus opening the possibility to compare aircraft concepts with different configurations (tube-and-wing, blended wing body, etc.) and propulsion architectures at a conceptual design-level
- Simplified turbofan and turboprop models combined with historical data regressions for accurate engine performance analysis and fuel burn estimates
- A visualization toolbox to render drawings of an aircraft concept both inside and outside the aircraft analysis [17]

FAST includes many pre-built aircraft models and mission profiles for a user to run before creating their own, thus reducing the time required to proficiently use FAST for design studies. In addition to extensive documentation in the software package, a video tutorial series[†] is also available for users to better understand how to use FAST effectively.

This paper details the main features of FAST, how data-based and first-order physics-based models are combined to rapidly size an aircraft, and an example sensitivity study comparing an aircraft concept with different propulsion systems, advanced technologies, and operational strategies. The remainder of the paper is as follows. Section II highlights the main aircraft sizing/analysis features, and illustrates the inputs that a user must provide in order to analyze an aircraft. Section III describes the built-in regressions that estimate any unknown information about the candidate aircraft design using the historical aircraft database mentioned previously. Section IV describes the aircraft sizing process, including the workflow, assumptions, and simplifications made. Section V describes the energy-based mission analysis in detail and assumptions made in the segment analyses. Section VII demonstrates using FAST for a retrofit study on a commercial freighter aircraft. Section VIII summarizes the work performed thus far and provides recommendations for further improving FAST.

[*] https://github.com/ideas-um/FAST

[†] https://www.youtube.com/playlist?list=PLNbQSl1VumqhNHgNOq9oxm4_Toi4_7v3-

II. Software Design and User Inputs

Before delving into each module of FAST in Sections III through V, a complete Design Structure Matrix (DSM) illustrating FAST's computational procedure is provided in Fig. 1[‡]. All information that is fed-forward and fed-backward is denoted with a gray box in the DSM's upper and lower triangular, respectively. Each dark blue cell groups certain functionalities together, which are displayed in gray.

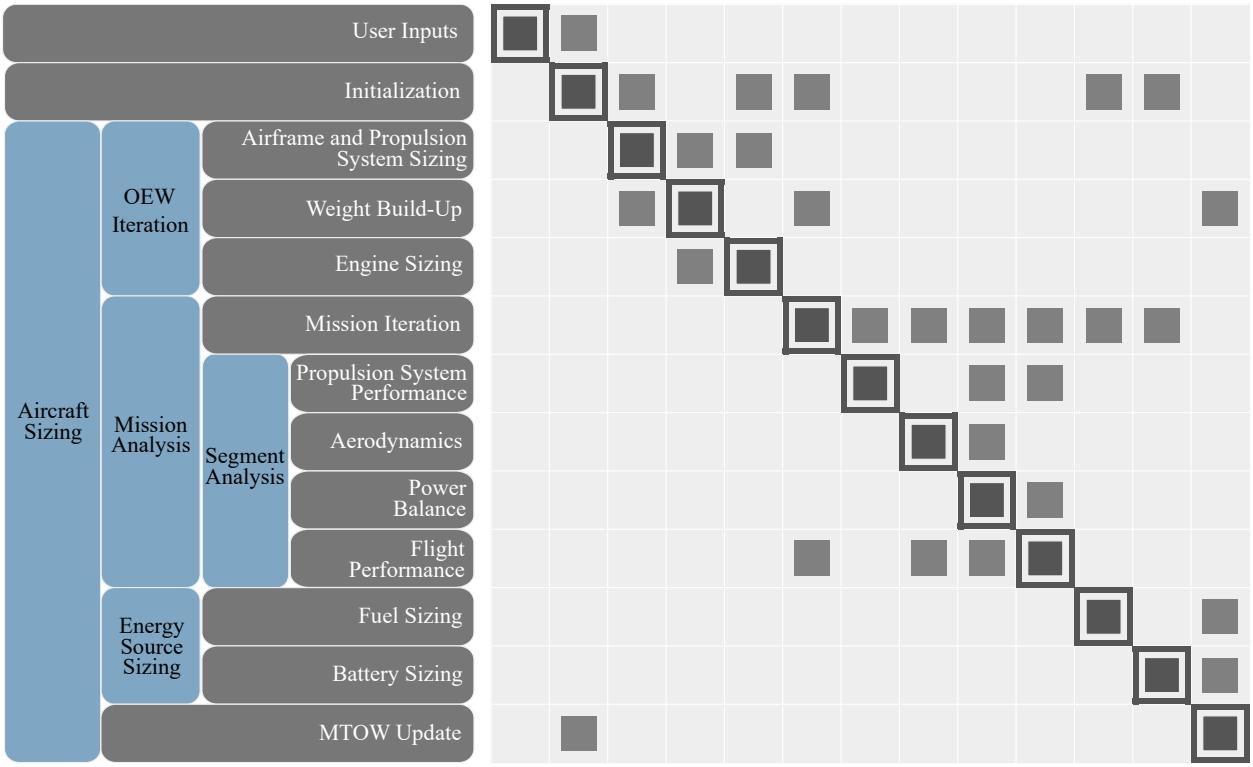

Fig. 1 FAST's overarching workflow

There are three main components to FAST's software: (1) an "Initialization" module that processes the user inputs, identifies any unknown values, and estimates the unknown values using regressions from historical data; (2) an "Aircraft Sizing" module that uses a *fixed* set of point performance parameters to size the airframe and propulsion system; and (3) a "Mission Analysis" module that calculates the mission performance, including the energy required to fly the prescribed mission.

The three user inputs are: (1) an aircraft specification file; (2) a mission profile; and (3) run settings (options) on how FAST should analyze the aircraft design at-hand. In this paper, only the aircraft specification file and mission profile inputs are reviewed – the run settings are not explained for brevity but can be reviewed in the documentation for FAST[§]. These required inputs are condensed into two files – an "Aircraft Specification" file, which also includes the run settings, and a "Mission Profile Specification" file – each of which is generated as a Matlab `.m` file.

A. Aircraft Specification File

The Aircraft Specification File defines all of the aircraft's design parameters, top level aircraft requirements (TLARs), and propulsion system architecture and operation. Every Aircraft Specification File outputs a data structure for the aircraft design, named `Aircraft`, with a sub-structure for all of the aircraft specifications, named `Specs`. The aircraft specifications are grouped into disciplinary sub-structures:

- `TLAR:` essential information about the aircraft being designed, such as the payload, aircraft class (turbofan or turboprop), EIS date, and cruise speed

[‡]All DSMs in this paper were created using OpenMDAO [18].

[§]`https://github.com/ideas-um/FAST/tree/main/%2BAircraftSpecsPkg`

- `Performance:` for information about the design range, takeoff/cruise altitudes and airspeeds, and the maximum rate-of-climb
- `Aero:` for all aerodynamic parameters such as the lift-drag ratio during climb, cruise, and descent
- `Weight:` for the aircraft- and component-based weights such as maximum takeoff weight (MTOW), operational empty weight (OEW), block fuel, engines, and electrical components
- `Propulsion:` for the aircraft's propulsion architecture, number of engines, and thrust-weight ratio (for turbofan-powered aircraft)
- `Power:` for the aircraft's power management strategy (how the propulsion system is operated during flight, particularly for electrified aircraft or engine-failure simulations), gravimetric specific energy of the energy sources used onboard the aircraft, and power-weight ratio (for turboprop-powered aircraft)

An example of the aircraft specification file is provided in Fig. 2[¶]. The example lists the parameters used to define a single aisle aircraft carrying 150 passengers for a 2,150 nmi design range. Notice that this aircraft specification only contains five user inputs. In fact, only the aircraft class (`TLAR.Class`), number of passengers (`TLAR.MaxPax`), design range (`Performance.Range`), and the propulsion architecture (`Propulsion.Arch.Type`) are required by FAST. All of the remaining aircraft specifications are determined using historical data and regressions described in Section III. To showcase all of the available user inputs, a comprehensive list is provided in Appendix IX.A. The run settings (mentioned previously) are also included in the Aircraft Specification File. A full listing of the available run settings is provided in Appendix IX.C.

```
%% TOP-LEVEL AIRCRAFT REQUIREMENTS %%
%%%%%%%%%%%%%%%%%%%%%%%%%%%%%%%%%%%

% entry to service year
Aircraft.Specs.TLAR.EIS = 2016;

% aircraft class
Aircraft.Specs.TLAR.Class = "Turbofan";

% approximate number of maximum passengers
Aircraft.Specs.TLAR.MaxPax = 150;


%% VEHICLE PERFORMANCE %%
%%%%%%%%%%%%%%%%%%%%%%%%

% design range (m)
Aircraft.Specs.Performance.Range = ...
    UnitConversionPkg.ConvLength(2150,'naut mi','m');

%% PROPULSION %%
%%%%%%%%%%%%%%%%

% propulsion architecture
Aircraft.Specs.Propulsion.Arch.Type = 'C';
```

Fig. 2 Example aircraft specification

1. Propulsion Architecture and Operation

The propulsion architecture and operational strategies are defined under the `Propulsion` sub-structure using the methodology from Cinar et al. [20]. In this methodology, power flows between components in the propulsion architecture are represented using matrices – a short description is provided here for the reader's understanding. The components in a propulsion system are divided into thrust sources (TS – components that generate thrust such as fans or propellers), power sources (PS – components that generate power such as a turboshaft engine or electric motor),

[¶]All figures generated from Matlab code were formatting for publication using `mcode` [19].

and energy sources (ES – components that store energy such as kerosene fuel or batteries). Three matrices, known as "Interdependency Matrices", are used to establish the connections between thrust, power, and energy sources: (1) B_{TSPS} shows the connections between thrust and power sources; (2) B_{PSPS} shows the connections between driven and driving power sources; and (3) B_{PSES} shows the connections between power and energy sources. These matrices can only contain values of 1 (to indicate a connection exists) or 0 (to indicate a connection doesn't exist). A series-hybrid propulsion architecture is provided in Fig. 3 as an example, in which "ES", "PS", and "TS", represent energy, power, and thrust sources, respectively.

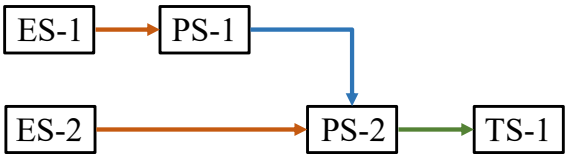

Fig. 3 Series-Hybrid propulsion architecture

In the series-hybrid architecture, there are two energy sources, two power sources, and one thrust source. The Interdependency Matrices are:

$$B^{A}_{\text{TSPS}} = \begin{bmatrix} 0 & 1 \end{bmatrix}$$

$$B^{A}_{\text{PSPS}} = \begin{bmatrix} 1 & 0 \\ 1 & 1 \end{bmatrix}$$

$$B^{A}_{\text{PSES}} = \begin{bmatrix} 1 & 0 \\ 0 & 1 \end{bmatrix}$$

B_{TSPS} is 1-by-2 to represent that there is one thrust source and two power sources. There is a 1 in the first row and second column because PS-2 is connected to TS-1. Since PS-1 is not connected to TS-1, there is a 0 in the first row and first column. B_{PSPS} is 2-by-2 to represent that there are two power sources. Since the power sources are assumed to power themselves, the diagonal of B_{PSPS} is always filled with ones. Also, in this architecture, PS-1 powers PS-2, which is why the second row and first column of B_{PSPS} also contains a 1. Lastly, B_{PSES} is 2-by-2 to represent that there are two power sources and two energy sources. The diagonal elements contain 1 because ES-1 is connected to PS-1 (first row, first column) and ES-2 is connected to PS-2 (second row, second column).

Similar matrices can be developed to show the power flow during operation. Instead of filling the matrices with ones and zeros, power splits – defined as the ratio of supplied power to total input power – are used to fill the entries. An example of these are:

$$B^{\lambda}_{\text{TSPS}} = \begin{bmatrix} 0 & 1 \end{bmatrix}$$

$$B^{\lambda}_{\text{PSPS}} = \begin{bmatrix} 1 & 0 \\ 0.6 & 1 \end{bmatrix}$$

$$B^{\lambda}_{\text{PSES}} = \begin{bmatrix} 1 & 0 \\ 0 & 0.4 \end{bmatrix}$$

For this example, PS-1 provides 60% of PS-2's input power and ES-2 provides the remaining 40%. Similarly, ES-1 provides 100% of PS-1's power and PS-2 provides 100% of TS-1's power.

B. Mission Profile Specification File

The Mission Profile Specification File is used to define a segment-based mission profile, or flight trajectory, for the aircraft being analyzed. An example of this is provided in Fig. 4. A comprehensive list of all inputs for the Mission Profile Specification File is provided in Appendix IX.D.

```
%% DEFINE THE MISSION TARGETS %%
%%%%%%%%%%%%%%%%%%%%%%%%%%%%%%%%

% define the targets (in m or min)
Mission.Target.Valu = [3981800;  45];

% define the target types ("Dist" or "Time")
Mission.Target.Type = ["Dist";  "Time"];


%% DEFINE THE MISSION SEGMENTS %%
%%%%%%%%%%%%%%%%%%%%%%%%%%%%%%%%

% define the segments
Mission.Segs = ["Takeoff"; "Climb"; "Cruise"; "Descent"; "Landing"];

% define the mission id (segments in same mission must be consecutive)
Mission.ID   = [        1;       1;        1;         1;         1];

% define the starting/ending altitudes (in m)
Mission.AltBeg = [     0;     0;  10668;  10668;   1524];
Mission.AltEnd = [     0; 10668;  10668;   1524;      0];

% define the climb rate (in m/s)
Mission.ClbRate = [   NaN;    NaN;    NaN;    NaN;    NaN];

% define the starting/ending speeds (in m/s or mach)
Mission.VelBeg  = [     0;   72.0;   72.0;   72.0;  102.9];
Mission.VelEnd  = [  72.0;   0.78;   72.0;  102.9;      0];

% define the speed types (either "TAS", "EAS", or "Mach")
Mission.TypeBeg = ["TAS";  "TAS"; "Mach"; "Mach"; "TAS"];
Mission.TypeEnd = ["TAS"; "Mach"; "Mach";  "TAS"; "TAS"];
```

Fig. 4 Excerpt from a mission profile specification

Each mission profile is comprised of one or more mission targets – a distance- or time-based value that must be flown by the aircraft – and are specified in the `Mission.Target.Valu` field. The distance- and time-based targets are specified in the `Mission.Target.Type` field as either "Dist" or "Time", respectively. Multiple mission targets can be provided in a single Mission Profile Specification File, which is useful for flying an aircraft's design and reserve missions while sizing. For the example in Fig. 4, the design mission is a distance-based target (fly 3,981,800 m) and the reserve mission is a 45-minute loiter.

Each mission is comprised of multiple segments: takeoff, climb, cruise, descent, and landing. While building a mission, note that an unlimited number of climb and descent segments can be included, but only one cruise segment per mission target can be included. This is because the cruise segment's length is iterated over to reach the desired mission target. Additionally, the first mission segment in the first mission target can be a takeoff segment and the last mission segment in the last mission target can be a landing segment. In Fig. 4, the example shows the first few segments in the design mission. The mission segments are arranged in chronological order, as shown in the `Mission.Segs` field.

In addition to arranging the segments, each one must have its own mission identification (ID) in the `Mission.ID` field to indicate which mission the segment should be included in. After the mission segments and IDs are listed, the boundary conditions for each segment must be provided:

- `Mission.AltBeg` and `Mission.AltEnd`: the initial and final altitudes flown in the segment, respectively.
- `Mission.ClbRate`: the rate-of-climb/descent within that segment. This is only used for the climb, cruise, and descent segments. The rate-of-climb/descent is an optional parameter. If it is specified, then FAST will force the aircraft to climb/descend at the given rate. If it is not specified (as done in the example with `NaN`), then FAST will vary the rate-of-climb/descent to ensure that the aircraft can fly without exceeding the power available from the

propulsion system.

- `Mission.VelBeg` and `Mission.VelEnd`: the initial and final airspeeds flown in the segment, respectively. These can be provided as a true airspeed, equivalent airspeed, or Mach Number.
- `Mission.TypeBeg` and `Mission.TypeEnd`: the type of initial and final airspeeds that were provided in the previous two fields, respectively. This is done by specifying a true airspeed as "TAS", an equivalent airspeed as "EAS", or a Mach Number as "Mach".

Every Mission Profile Specification File returns a structure containing the mission targets and information about each of the mission segments in the `Aircraft.Mission.Profile` sub-structure. Also, notice that this example mission profile was specified with hard-coded values. Should the user desire, they can represent the mission profile parametrically by using the variables provided in the aircraft specification file (like the design range, cruise altitude, or cruise speed). Specifying the mission parametrically is useful for flying a similar mission profile while using different aircraft specifications for the design range and takeoff/cruise altitudes/airspeeds.

Now that both inputs have been discussed, Section III explores how FAST parses the inputs, identifies values not provided by the user, and fills in those unknown values using Gaussian Process Models. Emphasis is placed on the Gaussian Process Models rather than the input parsing.

III. Historical Data and Regressions

As seen in discussed in Section II.A (and in Appendix IX.A), there are dozens of inputs that a user could provide. FAST only requires that four inputs be provided, as shown previously in Fig. 2. During early-phase conceptual design, the user is not expected to know all of the aircraft's design parameters. To estimate the necessary aircraft design parameters for FAST to run, the built-in regressions and technology regressions (detailed in [16]) predict any unknown values that the user does not provide based on the other given inputs. The regressions are housed in FAST's initialization module, as shown in Fig. 5, which provides a high-level overview of the pre-processing prior to analyzing the candidate aircraft design. In this DSM, note that: (1) orange cells represent user-prescribed inputs; (2) turquoise cell represents a major functionality in FAST and encapsulates all of its inputs (in dark green/blue) and outputs (in light green/blue).

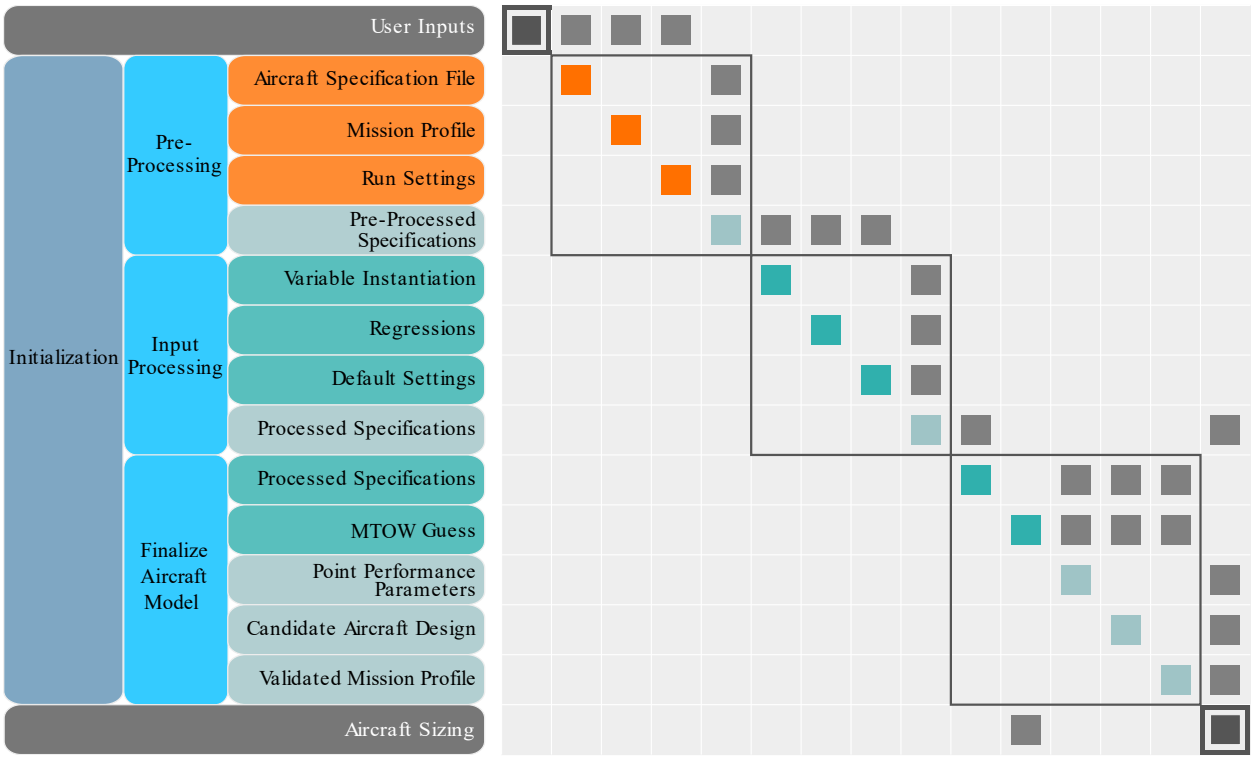

Fig. 5 Initialization module within FAST

The regressions were developed by gathering data from over 450 aircraft that were previously manufactured and flown. All of the data for the historical aircraft database were gathered from: (1) Type Certificate Data Sheets (TCDS) published by the FAA and European Union Aviation Safety Agency; (2) Airport Planning Manuals; or (3) the aircraft manufacturer's website. Information about the aircraft's designation, engines, payload, flight envelope, fuel, dimensions, and cabin crew were all collected. Some examples of the collected parameters are: certification date, number of engines on the aircraft, design range, maximum passenger capacity, MTOW, OEW, maximum operational Mach Number, and wingspan, to name a handful. All of the information collected in the database then drives the regressions to predict the design parameters for the aircraft design provided by the user. The regressions are created in real-time using Gaussian Process Models (GPMs). The inputs to the GPMs are the aircraft's EIS year, design range, and maximum payload, in addition to any additional parameters the user may have provided. From this information, the GPM will create a regression to determine the unknown aircraft parameters in the candidate design, as explained by [16]. Some quantities that can be predicted by the regressions are the aircraft's MTOW, cruise flight conditions, thrust- or power-weight ratio, wing loading, and fuselage length. Also, during the aircraft sizing process, the regressions are used to estimate the airframe and propulsion system weights.

In addition to the regressions that predict any unknown aircraft parameters, FAST also contains technology projections to predict key performance parameters associated with electrified aircraft components. The technology projections are represented by sigmoid curves and are used to predict the past, present, and future gravimetric specific energy for a battery and the power-weight ratio for an electric motor. Only two inputs are required for these projections – the aircraft's EIS year and its class (whether it is powered by a turbofan or turboprop engine).

IV. Aircraft Sizing

In the aircraft sizing module, the airframe, propulsion system, and energy sources are sized. The workflow associated with the aircraft sizing module is illustrated in Fig. 6. The "OEW Iteration" block sizes the airframe and propulsion system. Then, the mission analysis is executed to determine the required energy to fly the mission. Once the required energy is known, the "Energy Source Sizing" block sizes the energy sources (fuel, battery, etc.). This section reviews each of these blocks in greater detail, along with the respective calculations used in FAST.

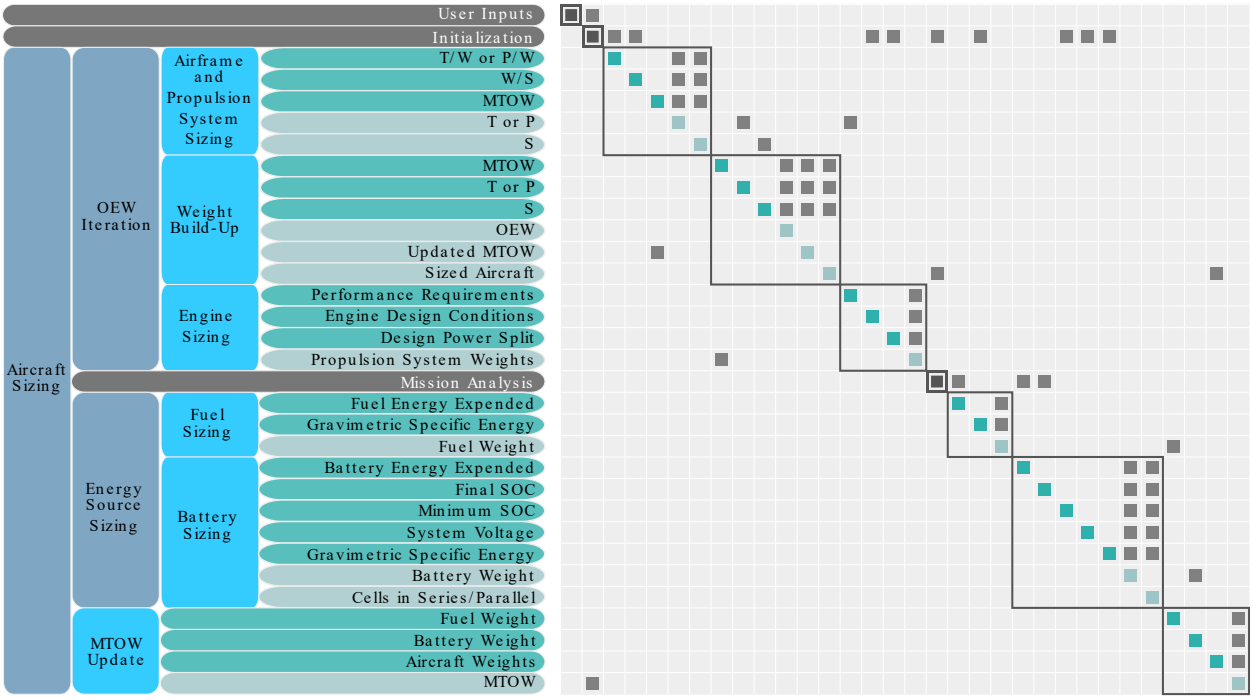

Fig. 6 Aircraft sizing module within FAST

A. Airframe and Propulsion System Sizing

The first sizing iteration estimates the airframe and propulsion system weights. A three-step process is used: (1) size the wing and propulsion system; (2) estimate the airframe and propulsion system component weights; and (3) update MTOW. FAST assumes that a feasible combination of point performance parameters (thrust- or power-weight ratio and wing loading) is provided by the user or the historical regressions. Since FAST does not currently generate constraint diagrams, the point performance parameters *remain fixed* while sizing the aircraft.

To size the wing, Eq. 1 is used, and is simply the quotient of MTOW and the wing loading. To size the propulsion system, the sea-level static (SLS) thrust (or power) is obtained using Eq. 2 or 3, depending on whether a turbofan or turboprop aircraft is being sized, respectively. The turbofan/turboprop engines are sized using a gas-turbine engine model, as described in Section VI.

$$S = \text{MTOW} / \left(\frac{W}{S} \right) \tag{1}$$

$$\mathcal{T}_{\text{SLS}} = \left(\frac{\mathcal{T}}{W} \right) \text{MTOW} \tag{2}$$

$$P_{\text{SLS}} = \left(\frac{P}{W} \right) \text{MTOW} \tag{3}$$

After these values are computed, the airframe weight is estimated using the historical regressions built within FAST. For turbofan aircraft, the airframe weight is estimated by inputting the wing area, SLS thrust, EIS year, and MTOW into a GPM. For turboprop aircraft, the airframe weight is estimated by inputting the MTOW into a linear regression.

Next, the propulsion system components are sized and their weights are estimated. Recall that the SLS thrust/power was already computed using Eqs. 2 or 3. Using these values, each component in the propulsion system is sized based on the SLS thrust/power and design power splits provided by the user. The power splits to size the components in the propulsion system are defined using the TSPS and PSPS matrices developed by Cinar et al. [20] (outlined in Section II.A.1), and allows for *any* propulsion architecture to be represented, regardless of how many engines, electric motors, etc. are included in the design. After the thrust/power is propagated to each component in the propulsion system, the weight for each component in the propulsion system is estimated. For any turbofan or turboprop engine, its weight is estimated by inputting its maximum SLS thrust or power, respectively, into a GPM. For any electric motor, its weight is estimated by Eq. 4. The electric motor's power-weight ratio can either be specified by the user, or is estimated by the historical regressions/projections based on the EIS year provided.

$$W_{\text{EM}} = \frac{P_{\text{EM}}}{(P/W)_{\text{EM}}} \tag{4}$$

Lastly, the aircraft's MTOW is updated by adding the weights in Eq. 5 together. This four-step process is a Fixed Point Iteration [21], and repeats itself until converging on MTOW.

$$\text{MTOW} = W_{\text{Airframe}} + W_{\text{Propulsion System}} + W_{\text{Crew}} + W_{\text{Payload}} + W_{\text{Energy Sources}} \tag{5}$$

B. Energy Source Sizing

The energy source sizing is performed after the mission analysis, as illustrated in Fig. 6, and computes how much fuel or battery must be carried by the aircraft to fly the design mission. Two different approaches are used to estimate the weight of the fuel (energy-based) and battery (energy- and power-based) to be carried on the aircraft.

1. Fuel Sizing

For this section, a fuel is defined as a substance that would be pumped into a storage tank on the aircraft, such as kerosene or hydrogen. To determine the fuel weight that must be carried on the aircraft, the energy expenditure, E_{fuel}, allocated to the fuel is divided by its gravimetric specific energy, e_{fuel}, as listed in Eq. 6. In other words, a fuel is only sized for its energy requirements.

$$W_{\text{fuel}} = \frac{E_{\text{fuel}}}{e_{\text{fuel}}} \tag{6}$$

Currently, the fuel sizing only considers the energy expenditure and does not consider the weight of the tanks to hold the fuel. While this is a reasonable estimate for aircraft using kerosene as its primary fuel source, it may not be a reasonable assumption for hydrogen-powered aircraft, which require much heavier fuel tanks. To remedy this, the authors suggest adding a calibration factor on the airframe weight to indicate that the larger fuel tanks will make the airframe heavier than expected.

2. Battery Sizing

The battery sizing accounts for both energy and power requirements. In FAST, the battery is built by arranging Lithium-ion cells in series (to obtain a desired system voltage) and in parallel (to obtain a desired power output). FAST assumes that each battery cell has a maximum capacity, $Q_{\max}$, and maximum voltage, $V_{\max}$, of 2.6 Ah and 3.6 V, respectively. In order to run the battery sizing module, the user must specify the number of battery cells in series and in parallel as an initial guess in the Aircraft Specification File. The number of battery cells in series remains fixed while sizing the aircraft, which corresponds to a fixed system voltage. In contrast, the number of battery cells in parallel changes to meet the power demands from the design mission. Unless the user specifies otherwise, the battery's initial state of charge (SOC) is assumed to be 100%. Aside from sizing for the maximum power required, it is also sized to ensure that its final SOC remains at or above 20%. The lower bound of 20% is applied because the battery could become permanently damaged if it is discharged any further [22].

Before sizing the battery, two checks are performed after the mission is flown. The first check ensures that the battery's final SOC is not less than 20%. Depending on how much battery energy was expended, the excess/lack of battery charge, ΔSOC, is computed to show how much energy must be added/removed from the battery. Then, Eq. 7 recomputes the required number of cells in parallel [22].

$$N_{\text{par,SOC}} = \left\lceil \frac{Q_{\text{batt}} + (\Delta\text{SOC})\, Q_{\max} N_{\text{par}}}{Q_{\max}} \right\rceil \tag{7}$$

The second check is to ensure that the C-rate, or battery's discharge rate, is not too large. The C-rate is defined in Eq. 8. FAST assumes a maximum C-rate of 5. If the C-rate is too high, additional cells must be added to ensure that the battery does not discharge too rapidly. To compute the number of cells in parallel required to meet this condition, Eq. 9 is used.

$$\text{C-rate} = \frac{\text{Power Required}}{\text{Total Energy}} \tag{8}$$

$$N_{\text{par,C-rate}} = \left\lceil \frac{\text{Maximum C-rate}}{\text{Maximum Allowable C-rate}} \right\rceil N_{\text{par}} \tag{9}$$

Now that the checks have been performed, the battery is resized. The number of cells in parallel is selected based on the two checks mentioned previously. Equation 10 shows that the number of cells in parallel is selected based on the more demanding sizing requirement (ensuring a minimum 20% SOC or maximum allowable C-rate of 5) [22]. After the number of parallel cells in the battery is updated, the battery's weight is recomputed, as shown in Eq. 11. Note that N_{ser} represents the number of battery cells in series and e_{batt} represents the battery's gravimetric specific energy.

$$N_{\text{par,new}} = \max\left(N_{\text{par,SOC}}, N_{\text{par,C-rate}}\right) \tag{10}$$

$$W_{\text{batt,new}} = 3600 V_{\max} Q_{\max} N_{\text{ser}} N_{\text{par,new}} / e_{\text{batt}} \tag{11}$$

Since FAST is a rapid aircraft sizing tool, there also may be instances in which the user only wants to size the battery for energy, not power requirements, especially if little is known about the aircraft during the conceptual design phase. In this case, the battery sizing module does not need to be run and the user can refrain from specifying the number of battery cells in series and parallel. Instead, the new battery weight ($W_{\text{batt,new}}$) will be computed using Eq. 12, and solely depends on the energy expended by the battery (E_{batt}) during the design mission.

$$W_{\text{batt,new}} = \frac{E_{\text{batt}}}{e_{\text{batt}}} \tag{12}$$

V. Mission Analysis

In the mission analysis, the user-prescribed mission profile is flown and computes the energy required to fly. The mission analysis informs the energy source sizing, as discussed previously in Section IV.B. The workflow for the mission analysis is illustrated in Fig. 7.

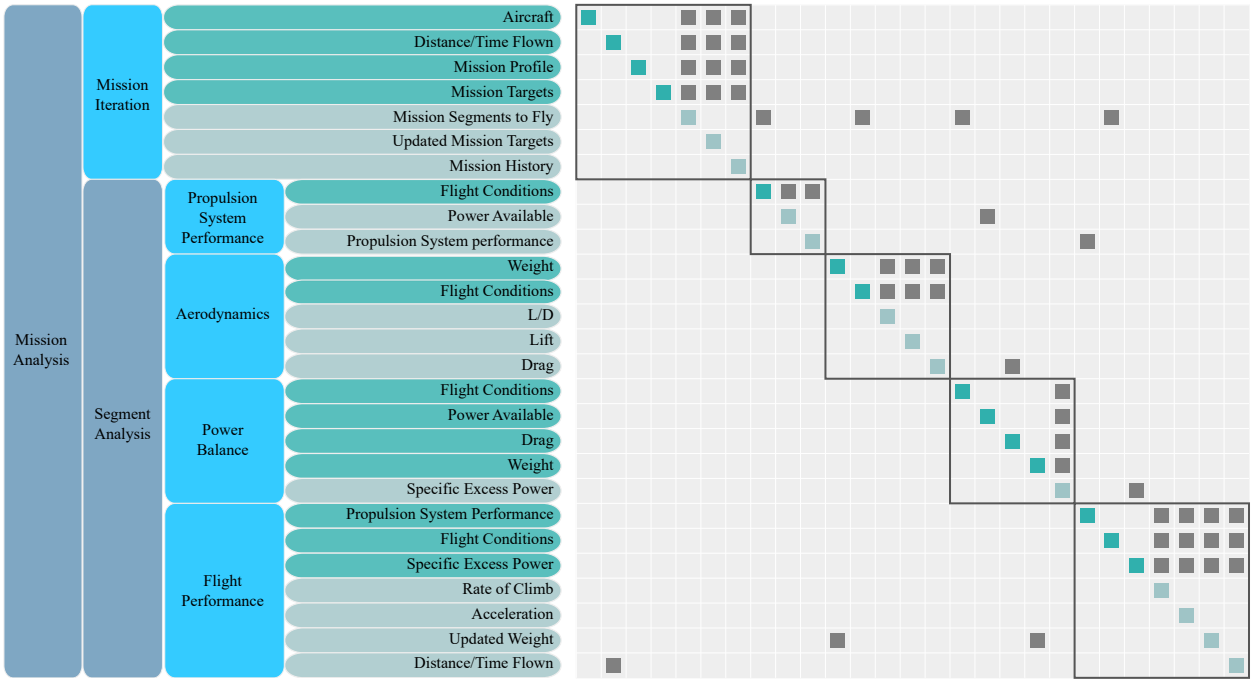

Fig. 7 Mission analysis module within FAST

Within the mission analysis, there are two groups of computations performed: (1) the mission iteration; and (2) the segment analysis. The mission iteration ensures that the (distance- or time-based) mission targets are achieved by performing a fixed-point iteration over the distance/time of the cruise segment. In the segment analysis, the aircraft flies the prescribed segments (takeoff, climb, cruise, descent, and landing) specified by the user. For this paper, the mission iteration is not discussed any further because it is only used to converge on the necessary cruise distance/time to match the mission target, and is not central to estimating the energy required to fly the mission. Instead, the computational procedure for the segment analysis and underlying assumptions within each segment are discussed in detail, which are essential for estimating the energy required to fly the mission.

There are four main functionalities in the segment analysis: (1) propulsion system performance; (2) aerodynamics; (3) power balance; and (4) flight performance. The propulsion system performance module estimates the power available as a function of altitude. The aerodynamics module predicts the drag force on the aircraft. Right now, this is achieved by assuming a constant lift-drag ratio in each segment. The power balance module computes how much power the aircraft can use to either climb or accelerate, namely, the specific excess power. The flight performance module computes how long it takes to fly the segment and returns the aircraft's rate of climb, acceleration, and energy expenditure. FAST's flight performance module uses an energy-based segment analysis that treats the aircraft as a point mass. As a result of this assumption, FAST allows for a rapid segment analysis and requires *no assumptions* about the aircraft's propulsion architecture, which is a core capability and distinguishes it from previous work in the field that developed propulsion architecture-dependent aircraft performance equations [23, 24].

This section reviews the: (1) computational procedure associated with FAST's segment analysis; (2) assumptions made in each segment; and (3) battery discharging model (when the user elects to use a detailed battery model). Section VI reviews propulsion system performance and engine modeling in greater detail.

A. Energy-Based Segment Analysis

All segments are evaluated using an energy-based analysis, which is shown in the "Segment Analysis" portion of Fig. 7. This approach assumes that the aircraft is a point mass and neglects any rigid body dynamics. The computational procedure for all segment analyses follows Algorithm 1, which is located in Appendix IX.E.

Before evaluating any segment, the trajectory is discretized into a set of control points by linearly interpolating between the initial and final altitudes and airspeeds. In the energy-based segment analysis, all instantaneous variables (power required, rate-of-climb, acceleration, etc.) are assumed constant between control points. After establishing the trajectory, the flight conditions are computed. The altitudes and airspeeds at each control point are used to compute the freestream density, ρ, and true airspeed, V_∞. Additionally, the aircraft is assigned an energy height, H_e, shown in Eq. 13. The energy height represents the aircraft's total mechanical energy normalized by its weight [25], and depends on both the aircraft's altitude and airspeed at each control point. These flight conditions (freestream density, true airspeed, and energy height) are used throughout the energy-based segment analysis to analyze the propulsion system performance, aerodynamics, and overall aircraft performance.

$$H_e = h + \frac{(V_\infty)^2}{2g} \tag{13}$$

Once the trajectory is established and flight conditions have been computed, the propulsion system performance is assessed. This involves computing the power available, $\mathcal{T}V_\infty$ for each component in the propulsion system. For turbofan aircraft using gas-turbine engines, the thrust is lapsed by the density ratio before multiplying by the true airspeed to obtain the power available, as shown in Eq. 14. For turboprop/piston aircraft using gas-turbine engines, the power is lapsed by the density ratio, as shown in Eq. 15. The lapse rate, m, varies amongst different turboprop/piston engines, and can be modified by the user in FAST's `EngineLapse` function. The power available from all non-air-breathing propulsion system components (electric motors/generators, fuel cells, etc.) remains constant with altitude – their power is not lapsed. Once the power available is known, the power available in each propulsion system component and the overall propulsion system performance is returned for later use.

$$\mathcal{T}V_{\infty,\text{turbofan}} = \left(\mathcal{T}_{\text{SLS}}\frac{\rho}{\rho_{\text{SLS}}}\right)V_\infty \tag{14}$$

$$\mathcal{T}V_{\infty,\text{turboprop/piston}} = P_{\text{SLS}}\left(\frac{\rho}{\rho_{\text{SLS}}}\right)^m \tag{15}$$

Next, the aerodynamic performance is evaluated. First, the lift is computed using Eq. 16, using the angle of attack based on the flight trajectory. Next, the drag is predicted using Eq. 17. Right now, FAST assumes a constant lift-drag ratio in the climb, cruise, and descent segments. The user may include more detailed or custom aerodynamic performance models as long as it computes the required aerodynamic performance outputs (lift, drag, and lift-drag ratio).

$$L = mg\cos(\alpha) \tag{16}$$

$$D = \frac{L}{(L/D)} \tag{17}$$

After the drag is computed, a power balance computes the specific excess power, P_s, as shown in Eq. 18. The specific excess power indicates how much power (normalized by the aircraft's weight) is available to either climb or accelerate after overcoming the requisite drag [25].

$$P_s = \frac{\mathcal{T}V_\infty - DV_\infty}{W} \tag{18}$$

Once the specific excess power is known, the aircraft's flight performance is evaluated. First, the time to fly between control points, Δt is computed. There are two ways to do this. One option requires the user to prescribe a given rate-of-climb/descent and the time to fly is computed using Eq. 19. Since the rate-of-climb/descent is fixed, all necessary excess power is used to climb/descend. Any remaining excess power is used to accelerate the aircraft. The maximum realizable acceleration at any control point is computed using Eq. 20. If the acceleration in the flight trajectory exceeds this, the true airspeeds at the current control point and all successive control points is re-computed accounting for the maximum realizable acceleration.

$$\Delta t = \frac{\Delta h}{(dh/dt)} \tag{19}$$

$$\left(\frac{dV}{dt}\right)_{\max} = \frac{(P_s - dh/dt)\, g}{V_\infty} \tag{20}$$

Another option to compute the time to fly is using Eq. 21, which depends on the specific excess power and does not require the user to prescribe a rate-of-climb/descent. (Absolute value bars are included to ensure that a positive Δt is returned, even during descent when ΔH_e is negative.) In some cases, using all of the specific excess power could return unrealistically large rates-of-climb/descent. If this occurs, the rate-of-climb/descent is restricted to the maximum rate-of-climb/descent provided in the Aircraft Specification file, and not all of the excess power is used. Once the maximum rate-of-climb/descent is restricted, Eq. 19 is used to compute the time to fly at the points where the maximum rate-of-climb/descent was exceeded. However, Eq. 20 is not required because not all of the excess power is being used – there will be enough power to accelerate and follow the given trajectory.

$$\Delta t = \left|\frac{\Delta H_e}{P_s}\right| \tag{21}$$

Once the time to fly is computed, the rate-of-climb and acceleration are updated using Eqs. 22 and 23, respectively. Using these quantities, the power required to fly that flight trajectory is computed using Eq. 24. This equations states that, in order to keep flying, the aircraft must generate enough power to overcome drag, climb, and accelerate [22].

$$\frac{dh}{dt} = \frac{\Delta h}{\Delta t} \tag{22}$$

$$\frac{dV_\infty}{dt} = \frac{\Delta V_\infty}{\Delta t} \tag{23}$$

The power required at the aircraft-level, found from Eq. 24, is propagated through the propulsion system to find the power required at each power source[‖], and is the same as was discussed in Section IV.A. Component models for the gas-turbine engine, electric motor/generator, etc., are then used to predict the power required that must be provided by the energy sources, $P_{\text{req, ES}}$, in order to power the aircraft. Lastly, the energy provided by each energy source onboard the aircraft is computed using Eq. 25 by accounting for how long it takes the aircraft to fly between successive control points. The energy required accumulates and is later used to size the energy sources, as explained in Section IV.B.

$$P_{\text{req}} = DV_\infty + W\frac{dh}{dt} + \frac{1}{2}mV_\infty\frac{dV_\infty}{dt} \tag{24}$$

$$E_{\text{req, ES}} = \sum_{i=1}^{n-1} \left(P_{\text{req, ES}}\right)^{(i)} \Delta t^{(i)} \tag{25}$$

B. Segment Analysis Assumptions

As previously mentioned in Section II.B, there are five segments that can be flown in FAST: takeoff; climb; cruise; descent; and landing. To simplify the analysis process for conceptual aircraft design, some key assumptions are made, and are provided in Tab. 1. The paragraphs that follow further describe the assumptions made in each segment.

The takeoff segment is approximated as one-minute long with a constant acceleration from a static position at the beginning of the runway to its takeoff speed, just as it rotates and lifts off from the runway. Since the aircraft is heaviest on takeoff, every power source in the propulsion architecture is assumed to operate at its maximum available power – a "full throttle" condition.

In the climb segment, the airspeeds are linearly spaced based on the final velocity type. For example, if the user sets the initial and final velocity types to "TAS" and "EAS", respectively, then the equivalent airspeeds will be linearly spaced in the climb segment. Similar to takeoff, every power source in the propulsion architecture is assumed to operate

[‖] As a reminder, readers interested in understanding how the thrust power is propagated along the powertrain should refer to Cinar et al. [20] for more information.

Table 1 Assumptions made in FAST's segment analyses

Assumption	Takeoff	Climb	Cruise	Descent	Landing
Fixed Time	✓	✗	✗	✗	✓
Constant Acceleration	✓	✗	✗	✗	✓
No ISA Temperature Deviation	✓	✓	✓	✓	✓
Constant L/D	✗	✓	✓	✓	✗
Linearly Spaced Altitudes and Airspeeds	✓	✓	✓	✓	✓
Maximum Power	✓	✓/✗	✗	✗	✗
Reverse Thrust	✗	✗	✗	✗	✓

at its maximum available power ("full throttle") to allow the aircraft to reach its cruise altitude quickly. However, if a rate-of-climb is prescribed, the power required may be less than the power available. In this case, the power sources provide only the necessary power to fly between the control points and do not operate at a "full throttle" condition.

The assumptions made in the descent segment are nearly identical to the climb segment. However, there are a few exceptions. The maximum descent rate is assumed to be 80% of the maximum rate-of-climb given in the aircraft specifications. Also, the lift-drag ratio is not scaled to account for flap deflections, landing gear extensions, and the like. In the event that no power is required while descending, it is assumed that a small amount of thrust/power is required, which is approximated as 5% of the SLS thrust/power, and shows that the engine is still generating some quantity of thrust/power at a very low throttle setting.

The landing segment is approximated as 30-seconds long with a constant acceleration from touchdown at its landing speed to a static position at the end of the runway. To account for reverse thrust, 30% of the power available is assumed to be used to bring the aircraft to a stop.

In future releases of FAST, some of the assumptions listed above will be removed from the code by creating more detailed models. For example, the constant lift-drag ratio assumption could be removed from the code by developing an elementary aerodynamic analysis to approximate the ratio instead. Additionally, more detailed takeoff and landing models that incorporate force balances would allow the fixed takeoff/landing time assumptions to be eliminated.

C. Battery Discharge

In the event that the user desires uses a "detailed battery" by prescribing the number of cells in series and parallel, a detailed battery discharging model is needed. A battery (dis)charging model was adapted from Tremblay and Dessaint [26] for a Lithium-Ion battery cell, and is shown in Eqs. 26 and 27. Table 2 lists all the variables used in the battery (dis)charging model.

$$V_{\text{discharge}} = E_0 - Ri - K\frac{Q}{Q - it}\left(it + i^*\right) + Ae^{-Bit} \tag{26}$$

$$V_{\text{charge}} = E_0 - Ri - K\frac{Q}{it - 0.1Q}i^* - K\frac{Q}{Q - it}it + Ae^{-Bit} \tag{27}$$

Currently, only battery discharge is used in FAST. However, battery charging will be useful in the future for power management strategies that charge a battery from operating a gas-turbine engine or windmilling from a propeller.

VI. Gas Turbine Modeling

A. Overview

FAST's engine modeling capability is a standalone feature that can size turbofan, turbojet, and turboprop engines, and evaluate their performance. Like the aircraft sizing module, an input specification file, known as the engine specification file, is required to describe the engine being sized. However, there are no regressions that fill in missing values for the engine specification files – all inputs must be provided. These inputs include the flight conditions (Mach number and

Table 2 Variables used in the battery (dis)charging model [26]

Variable	Description
V	Battery voltage as a function of time (V)
E_0	Battery constant voltage (V)
R	Battery internal resistance (Ω)
it	Battery capacity as a function of time (Ah)
K	Polarization Constant (Ω)
Q	Maximum battery capacity (Ah)
i^*	Filtered current (A)
A	Battery's exponential zone amplitude (V)
B	Battery's time constant $\left(\text{Ah}^{-1}\right)$

altitude), as well as information about the internal engine architecture (number of shafts, shaft speeds, gearing, etc.). A complete list of engine model variables is summarized in IX.B. The information from the engine specification file is passed to a sizing function which varies the engine size until the required thrust, power, or both (called "performance") are produced, described in Section VI.B. Regressions, discussed in Section III, are used to predict the engine weight and length. Off-design performance is evaluated using a numerical method as shown in Section VI.E.

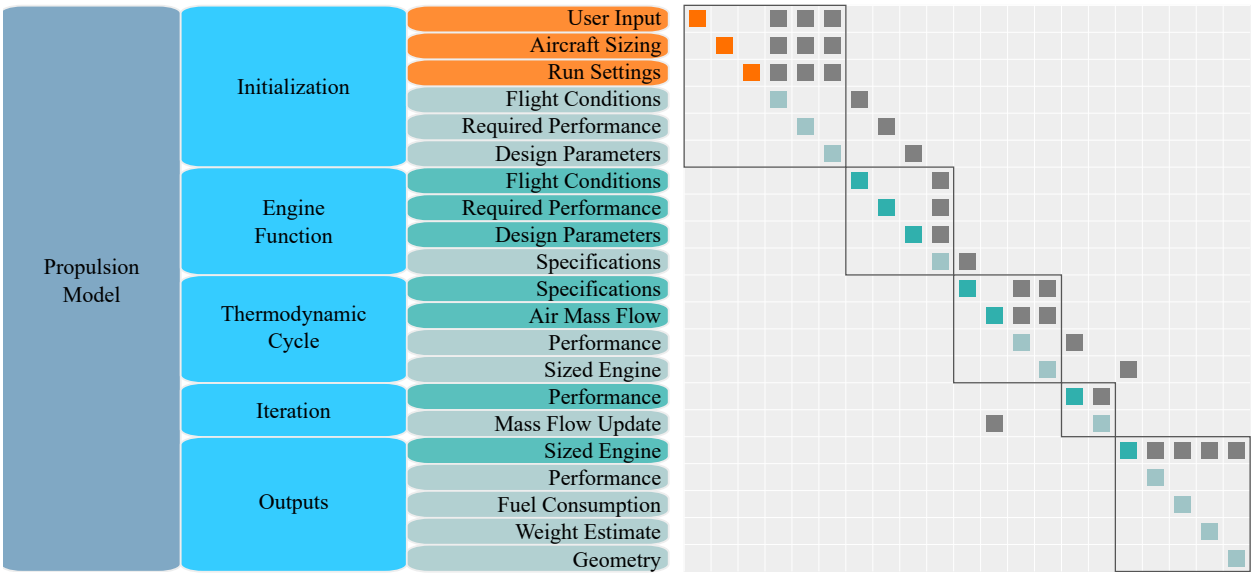

Fig. 8 Gas turbine sizing module within FAST

B. Thermodynamic Cycle

The thermodynamic cycle within the gas turbine model follows the procedure(s) outlined in canonical sources including Mattingly [27], Boyce [28], Walsh and Fletcher [29], and Saravanamuttoo [30]. The cycle model calculates the power turbine output (i.e., performance, as shown in Fig. 8) as a function of the air mass flow rate. A fixed point iteration on the air mass flow rate changes the engine size to generate the thrust/power requested by the user. A thermodynamic

"flow state", comprised of values such as pressure, temperature, Mach Number, flow area, etc. is stored at a location within each engine section or "station", illustrated by a station map shown in Tab. 3. This convention is shared between all types of gas turbine engines. If an engine does not have a component, it is simply ignored. For example, stations 1 through 2.6 would be identical for a turboprop engine with one compressor, since there is no fan, LPC, or IPC.

Table 3 FAST's engine station numbering convention.

Station Number	After	Before
0 or a	Streamtube	Inlet
1	Inlet	Fan
2	Fan	Splitter
2.1	Splitter (Core)	LPC
2.5	LPC	IPC
2.6	IPC	HPC
3	HPC	Bleeds
3.1	Bleeds	Combustion Chamber Diffuser
3.2	Combustion Chamber Diffuser	Combustion
3.9	Combustion	Turbine Diffuser
4	Turbine Diffuser	Cooling Air
4.1	Cooling Air	HPT
5	HPT	IPT
5.5	IPT	LPT
6	LPT	Core Nozzle
9	Core Nozzle	Core Exhaust
13	Splitter (Bypass)	Bypass Nozzle
19	Bypass Nozzle	Bypass Exhaust

By inputting the flight conditions (Mach Number, M, and an altitude which correlates to an air density, ρ, and an air temperature, T) and with a mass flow rate, $\dot{m}$, a stream tube area A is calculated according to Eq. 28, where R is the gas constant for air (287 J/kgK). FAST assumes air behaves as a thermally perfect gas (i.e. the air obeys the ideal gas law but the ratio of specific heats γ is *not* constant, and is a function of temperature). This assumption is discussed later in this section, where it is shown that this additional fidelity over a calorically perfect assumption comes at little additional computational complexity.

$$A_0 = \frac{\dot{m}}{\rho_0 M \sqrt{\gamma(T_0) R T_0}} \tag{28}$$

This stream tube is then diffused using the isentropic area relations until a desired Mach Number is reached. A default value of Mach 0.5 is used in FAST, but can be changed by a user if a different value is desired. In turbofans, the air then enters the "fan system". However, in turboprops, the air travels directly to a compressor. The fan system consists of a series of logical statements that parse the user inputs. FAST creates an engine architecture from the engine specification file, using information like the number of spools, the `GearRatio` value, and the `Boosted` value stored in the engine specification file. The `GearRatio` flag defines the ratio of RPMs between the fan itself and the fan turbine (defaults to 1 if unspecified), while the `Boosted` flag indicates whether additional compressor stages are added to the fan's shaft. Figure 9 provides examples of inputs and resultant engine architectures for a 2-spool engine. A 3-spool engine would look very similar aside from an additional intermediate pressure compressor-turbine pair between the high and low pressure shafts. A 1-spool architecture would remove the illustrated high pressure compressor-turbine pair. Currently, FAST cannot accommodate architectures outside of the 1-3 shaft range.

Based on the input engine architecture, overall pressure ratio (OPR), and fan pressure ratio (FPR), each compressor is assigned an individual compressor pressure ratio (CPR) it must accomplish according to Eq. 29. This assumption

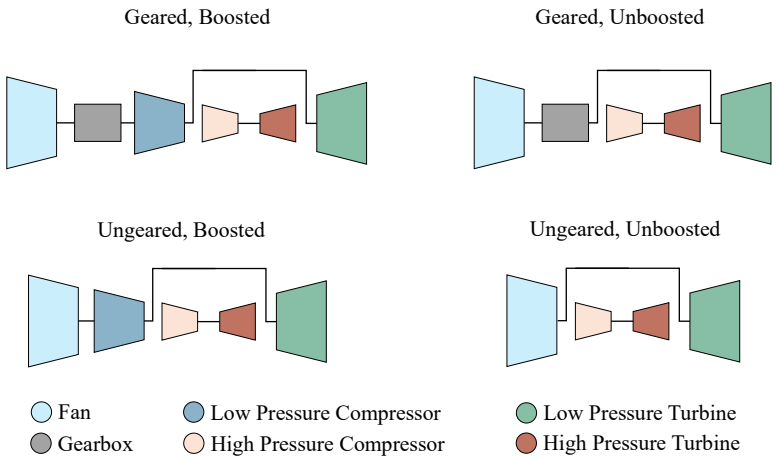

Fig. 9 Example architectures for a 2-spool turbofan engine in FAST.

assigns equal pressure rises among all compressors other than the fan. After passing through the fan, the air is split between core air and bypass air according to a specified bypass ratio.

$$\text{CPR} = \left(\frac{\text{OPR}}{\text{FPR}}\right)^{\frac{1}{N_{\text{Spools}}}} \tag{29}$$

The flow state is then passed through all the compressors (including the fan). Compressor components take an input flow state and output a modified version post-compression. The compressor components additionally document the changing annulus area as well as the work required to drive them at their set rotational speed (compressor RPMs are required as inputs in the specification file). Within a compressor, FAST iteratively adds compressor stages until the desired pressure ratio is achieved. FAST limits the maximum pressure ratio per stage within the compressor to 1.41, which prevents the program from designing excessively loaded compressor stages. The pressure ratio per stage, π, is used to calculate the temperature ratio in a given stage, τ, according to the isentropic relation given in Eq. 30.

$$\tau = \pi^{\frac{\gamma-1}{\gamma}} \tag{30}$$

The temperature ratio is applied to the compressor stage inlet temperature, yielding a stage outlet temperature. These two values act as the bounds for FAST to integrate the specific heat at constant pressure, yielding a specific work required to drive the current compressor stage. This value is scaled by the mass flow rate. Then, inefficiencies in the compression are modeled with a user specified adiabatic efficiency, such that the work the turbine will be required to produce is a set percentage higher than the actual work required to compress the air.

The $C_p(T)$ curve is fitted from historical data. This data is sourced from Urieli [31], who compiled previous work by Hilsenrath et al. [32] and Kyle [33] into an open-source online thermodynamics resource center. The raw data is fitted with a sigmoid curve to avoid extrapolating beyond the range of the given domain. The curve is described in Eq. 31, and illustrated alongside the raw data from Urieli [31] in Fig. 10a. The fitted curve has a coefficient of determination $R^2 = 0.9894$, showing that the fit is appropriate.

$$C_{p,\text{air}}(T) = \frac{233}{1 + \exp\left(-0.0048(T - 875)\right)} + 993 \tag{31}$$

The sigmoid shape assumption may under-predict the TSFC for engines which burn fuel at temperatures higher than 2000 K. Though it is important to be aware of this limitation, combustion temperatures much higher than 2,000 K are unrealistic as dissociation (not accounted for in FAST) and material properties often limit extremely high temperatures in practice, making it undesirable to design an engine at the conceptual level which operates at those temperatures.

Similar to the air, a C_p curve for JP-8 was fit using data from Xu et al. [34]. The results show a good fit, with a coefficient of determination $R^2 = 0.9815$. The curve is shown in Fig. 10b, and is fully described by Eq. 32. Equations 31 and 32 are both empirical relations, making it easy to compute the enthalpy rises as functions of temperature, which

increases the fidelity of the model over a calorically perfect model at little additional computational cost. However, due to the limits of the data, FAST defaults back to a calorically perfect model once the air exceeds the temperature domain of the data collected, and the value of C_p becomes constant.

$$C_{p,\text{JP-8}}(T) = \frac{4600}{1 + \exp\left(-0.0024(T - 500)\right)} + 100 \tag{32}$$

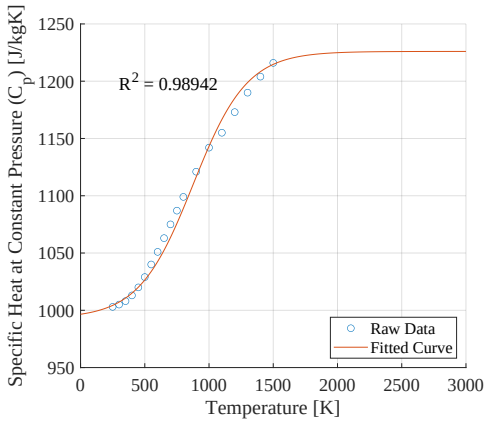

(a) Specific heat capacity of air at constant pressure given by [31], with FAST's curve fit and coefficient of determination

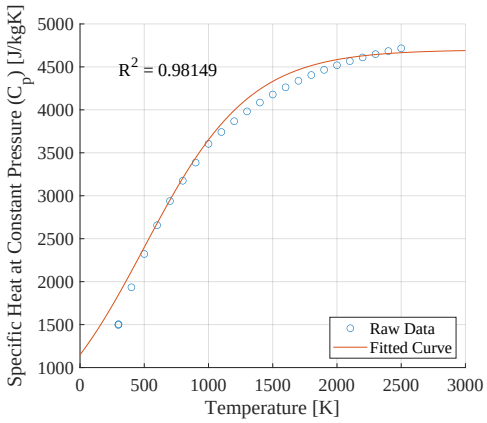

(b) Specific heat capacity of JP-8 at constant pressure given by [34], with FAST's curve fit and coefficient of determination

Fig. 10 Specific heat capacities for air and JP-8 with FAST's curve fits and coefficients of determination.

With compressor work calculated, the high pressure air has fuel added until the prescribed combustion temperature is reached, according to Eq. 33. Due to the form of Eqs. 31 and 32, their analytical anti-derivatives are easily found and allow for quick computation of Eq. 33. FAST assumes the following regarding combustion: a lower heating value LHV of JP-8 to be 43.17 MJ/kg; combustion chamber diffusers are flat walled diffusers with tailpipes and pressure loss behavior according to Mattingly's Eq. 9.41 [27]; and the combustion process yields an additional 5% stagnation pressure loss.

$$\dot{m}_{\text{fuel}} = \frac{\dot{m}_{3.2} \int_{T_{t,3.2}}^{T_{t,3.9}} C_{p,\text{air}}(T)}{\eta_{\text{Comb}} LHV_{\text{JP-8}} - \int_{T_{t,3.2}}^{T_{t,3.9}} C_{p,\text{JP-8}}(T)} \tag{33}$$

After combustion, the turbine(s) extract work based on a user-prescribed turbine efficiency and the required work the corresponding compressor requires. The turbine exit temperature is set in one of two ways depending on if the propulsion architecture uses thrust or power as its performance metric. If it uses thrust as the performance metric, the exit temperature is set using the C_p curve such that the integral from the inlet temperature drop to the exit temperature equals the amount of work required by the corresponding compressor. If it uses power as the performance metric, the exit temperature is set such that the pressure ratio across the turbine results in an exit pressure equal to ambient air pressure at the design altitude.

For some electrified propulsion architecture, the propulsion system performance module passes a value to the engine model representing an electrical power boost/siphon, which represents how much power is being provided/requested by the electrified portion of the propulsion architecture. This reduces/increases the power that the turbine is required to produce. The convention within FAST is: (1) positive electrical loads represent a supplemental power boost and reduce the engine's power demands; and (2) negative electrical loads represent a supplemental power siphon and add to the thrust producing loads, thus requiring the turbine to produce additional power. Equation 34 shows this convention for turbines with known work requirements while Eq. 35 shows the same for turbines with the goal of producing as much power as possible. The left arrow represents that work done *on* the turbine is positive. Additionally, to match this convention, a negative sign is needed in front of the integral in Eq. 35 to ensure that the output of the integration from high to low temperature is positive. As an example, a battery boosted takeoff would use a positive electrical work input,

reducing turbine demand. In contrast, a turboelectric propulsion architecture would require a negative input because the gas-turbine engine is powering an electric generator, which increases turbine demand.

$$W_{\text{Turbine}} = \frac{W_{\text{Compressor}} - W^{\leftarrow}_{\text{Electrical}}}{\eta_{\text{Turbine}}} \tag{34}$$

$$W_{\text{Turbine}} = \frac{-\dot{m}_{\text{inlet}} \int_{T_{t,\text{inlet}}}^{T_{t,\text{exit}}} C_{p,\text{air}}(T) - W^{\leftarrow}_{\text{Electrical}}}{\eta_{\text{Turbine}}} \tag{35}$$

$$\text{Where} \quad T_{t,\text{exit}} = T_{t,\text{inlet}} \left(\frac{P_{t,0}}{P_{t,4.1}} \right)^{\frac{\gamma-1}{\gamma}}$$

Stage loading is limited to 2 as suggested by Walsh and Fletcher [29]. The overall loading, ψ, is shown in Eq. 36, where ω is the turbine rotational velocity, R_p is the pitch line radius, and $W_{\text{Compressor}}$ and η_{Turbine} are the compressor work and turbine efficiency, respectively. The overall loading is divided by the stage limit, 2, and rounded up to the nearest whole number to determine how many stages are required.

The turbine RPM is set equal to the compressor or fan RPM which the turbine powers (multiplied by any gear ratios) and the pitch line turbine radius is assumed to be equal to the pitch line at the entrance to the turbine. Since the flow path area increases throughout the turbine, this is the most restrictive pitch line radius, and will result in lower than 2 individual stage loadings (which is desirable [29]). FAST also limits the number of turbine stages to 7, which is the practical limit found in most engines stored within FAST's databases.

$$\psi = \frac{W_{\text{Compressor}}}{\eta_{\text{Compressor}} (\omega R_p)^2} \tag{36}$$

After the number of stages is determined, each stage extracts energy from the airflow, "powering" the compressor and any additional electrical components requested by the propulsion architecture. At this point in the engine design process, the procedure splits according to the following:

Turbofans: All turbines in a turbofan architecture have their work output known, and thus use Eq. 34. After air passes through the turbines, the air in the core (and the bypass duct) are ideally expanded to atmospheric pressure at the design altitude, producing a thrust described by Eq. 37, where all $\dot{m}$ are mass flow rates and all u are velocities.

$$\mathcal{T} = \dot{m}_9 u_9 + \dot{m}_{19} u_{19} - \dot{m}_0 u_0 \tag{37}$$

This thrust is then output as the performance metric as mentioned in Sec. VI.A.

Turboprops/shafts: The turbines in a turboshaft architecture use Eq. 34 *except* if they are a free turbine, which will use Eq. 35. The work output from the free turbine is output as the performance metric mentioned in Sec. VI.A. If the turboshaft uses a single turbine to power both external thrust sources and its own compressor, the compressor work is subtracted from the turbine work before being reported as output power.

The performance metric is then output to the engine sizing iteration and the streamtube mass flow rate is modified until the performance matches that requested by the design specification while meeting any additional electrical demands.

C. Aircraft Sizing Interaction

The propulsion system interfaces with the mission analysis for the aircraft. Unlike processing the aircraft specification file, the engine model does not get processed in FAST – either a comprehensive engine specification file (all inputs defined) is coupled to the aircraft specification file under the appropriate field (`Aircraft.Specs.Propulsion.Engine`) or is initialized to `NaN`, allowing the aircraft specification parser to use GPM regressions to predict the values for an engine based on those used in similar aircraft.

If the aircraft is being sized, the weight of the engine is flexible and allowed to change during the analysis. The weight is computed at the sizing condition, which is assumed to be takeoff. If the aircraft is not being sized, the weight of the propulsion system is fixed.

Regardless of whether the aircraft is sized or not, the mission analysis requires a fuel burn at each control point. The current Mach number and altitude are passed to the engine model, as well as the required power or thrust for the desired

telemetry. The engine performance evaluates the fuel required per second to meet these requirements and passes the information back to the aircraft sizing function(s). If sizing the aircraft, the engine model also records internal engine geometry (flow path areas, station-wise pressures and temperatures, etc.).

A user can also evaluate an engine outside of FAST's aircraft analysis or model an existing engine which has not been included in the default engine specification file folder. Example engine specification function files are provided in FAST for both turbofan and turboprop engines. The associated documentation is comprehensive, and alongside the GPM documentation, should allow users to not only model any engine they desire, but to additionally use regressions to predict unknown engine design parameters.

D. Example

An example engine specification file is shown in Fig. 11, while an example output is shown in Fig. 12, enabled with an optional visualization feature (`Engine.Visualize = true`).

```
%% Design Point Values %%
%%%%%%%%%%%%%%%%%%%%%%%%%

% Design point Mach Number
% If SLS, enter 0.05
Engine.Mach = 0.05;

% Design point Altitude [m]
% If SLS, enter 0
Engine.Alt = 0;

% Overall Pressure Ratio
Engine.OPR = 40;

% Fan Pressure Ratio
Engine.FPR = 1.5;

% Bypass Ratio
Engine.BPR = 10;

% Combustion Temperature [K]
% If unknown, 2000 is a good guess
Engine.Tt4Max = 1800;

% Design point thrust [N]
Engine.DesignThrust = 1e5;
```

Fig. 11 Example engine specification excerpt (not representative of any existing engine)

E. Off-Design Engine Modeling

The following methodology only applies to turbofan engines because there is no data in the *ICAO Aircraft Emissions Databank* for turboprop/shaft engines. For estimating fuel consumption in turboprop/shaft engines in FAST, two key assumptions are made: (1) component efficiencies are constant with respect to performance requirements; and (2) component efficiencies are constant with respect to the throttle settings. This yields a linear response in fuel consumption with respect to output power (constant brake-specific fuel consumption with respect to output power). The effects of these assumptions are offset by tuning a fuel flow calibration factor and comparing the total fuel burn to literature values at a design mission.

For all engine types, FAST needs a way to calculate total power available from the gas turbines to ensure each mission segment is feasible with a given engine size. FAST currently uses an engine lapsing method presented in Anderson [25], and is shown in Eq. 38. This equation assumes the total performance available from the engine is an exponential function of the ratio of air density, ρ, at altitude to that at sea level. In FAST this exponent is $m = 1$ for

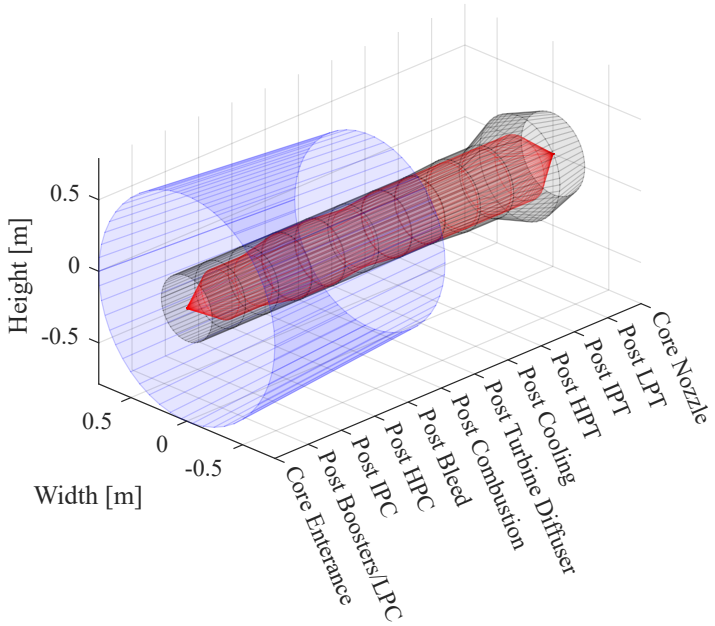

Fig. 12 Example engine model output with visualization enabled

turbofan engines and $m = 0$ for turboprops/shafts, but can be lapsed by the user.

$$\frac{\mathcal{T}}{\mathcal{T}_{SLS}} \quad \text{or} \quad \frac{P}{P_{SLS}} = \left(\frac{\rho}{\rho_{SLS}}\right)^m \tag{38}$$

1. Off-design Turbofan Engine TSFC Model Overview

The *ICAO Aircraft Emissions Databank* provides comprehensive data on turbofan engine fuel flow rates across four operational mission modes, as reported by engine manufacturers [35]. The power settings for these engines are designated at 100%, 85%, 30%, and 7%, representing the maximum power output for takeoff, climb-out, approach, and idle, respectively. To estimate the actual fuel consumption under different operational conditions, including thrust required and altitude, Sun et al. [36] proposed a polynomial function for predicting these fuel flow rates. The polynomial function for each turbofan engine utilizes three coefficients – C_{ff3}, C_{ff2}, and C_{ff1} – derived from a third-degree polynomial curve fit of the points provided in the databank, shown in Eq. 39. Additionally, a simplified linear correlation factor – $C_{ff,ch}$ – was introduced to account for discrepancies in the TSFC at SLS and cruise conditions at altitude, shown in Eq. 40. Combining Eqs. 39 and 40, the final fuel flow rate equation is provided in Eq. 41.

$$\dot{m}_{f,ICAO}(\mathcal{T}) = C_{ff3}\left(\frac{\mathcal{T}}{\mathcal{T}_0}\right)^3 + C_{ff2}\left(\frac{\mathcal{T}}{\mathcal{T}_0}\right)^2 + C_{ff1}\left(\frac{\mathcal{T}}{\mathcal{T}_0}\right) \tag{39}$$

$$\begin{aligned} C_{ff,ch} &= \frac{TSFC_{Cr} - TSFC_{SLS}}{h_{Cr}} \\ &= \frac{TSFC_{Cr} - \dot{m}_{f,\text{ICAO}}(\mathcal{T}_0)/\mathcal{T}_0}{h_{Cr}} \end{aligned} \tag{40}$$

$$\dot{m}_f(\mathcal{T}, h) = C_{ff3}\left(\frac{\mathcal{T}}{\mathcal{T}_0}\right)^3 + C_{ff2}\left(\frac{\mathcal{T}}{\mathcal{T}_0}\right)^2 + C_{ff1}\left(\frac{\mathcal{T}}{\mathcal{T}_0}\right) + C_{ff,ch} \times \mathcal{T} \times h \tag{41}$$

In these equations, $\dot{m}_{f,ICAO}(\mathcal{T})$ represents the fuel flow rate of an engine provided in the ICAO databank (kg/s); C_{ff3}, C_{ff2}, and C_{ff1} represent the coefficients for the polynomial function (kg/s); $\mathcal{T}$ and $\mathcal{T}_0$ represent the required thrust during flight and the maximum static thrust of the engine (kN), respectively; $C_{ff,ch}$ represents the correlation factor for the cruise altitude condition and has units of $\frac{kg}{s \times kN \times m}$; $TSFC_{CR}$ and $TSFC_{SLS}$ represent the thrust specific fuel consumption for cruise and sea-level conditions, respectively; and h_{CR} represents the aircraft's cruise altitude.

2. Turbofan Engine TSFC Model Validation

To evaluate the feasibility of the fuel flow equation presented in Eq. 41 [36], the coefficients in Eqs. 39 and 40 were estimated based on the ICAO databank and relevant literature [35, 37, 38], as detailed in Appendix IX.F. For the data analysis, four turbofan engines from different manufacturers were selected to demonstrate the accuracy of the third-degree polynomial curve fitting results compared to the ICAO databank for Eq. 39, shown in Fig. 13. The CF34-8E5, LEAP1A26, LEAP1B and Trent 772 are used onboard the ERJ175LR, A320neo, Boeing 737 Max 8 and A330, respectively. Figure 13 illustrates that the fuel flow results obtained from the fitted curves for different engines closely align with the values reported in the ICAO databank, indicating that the coefficients were accurately estimated. Additionally, the simplified linear correlation factor was calculated by Eq. 40 and relevant data of TSFC in cruise [36–38]. Figure 14 demonstrates that each engine type has varying correlation factor values, depending on its TSFC during cruise and sea level, and its design conditions. Even engines produced by the same manufacturer can display performance variations. Furthermore, Fig. 14 presents an average value of the simplified linear correlation factor, 6.8×10^{-7}, derived from the collected turbofan engines. This average value can be a default reference in cases where specific engine performance details are unavailable.

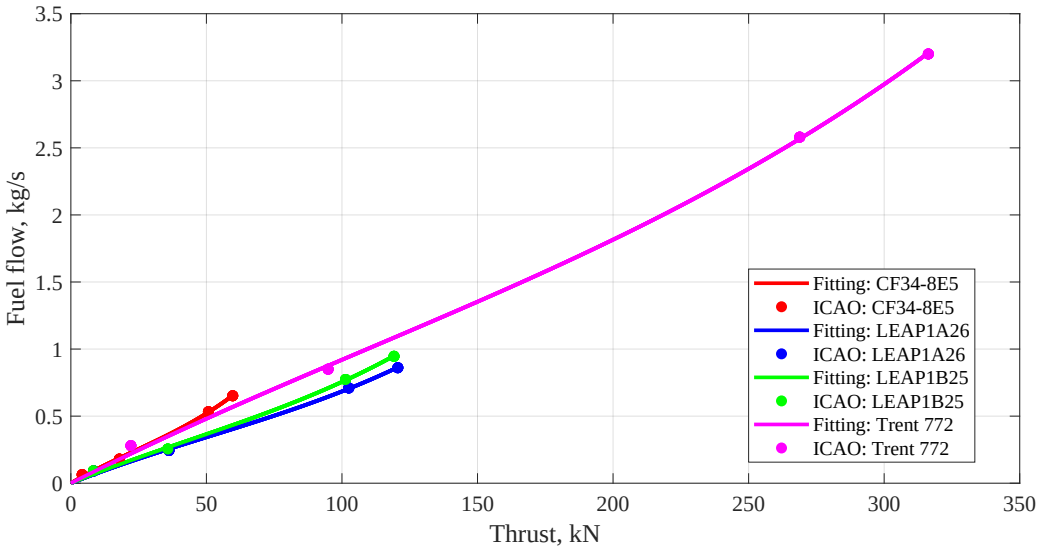

Fig. 13 Validation of the polynomial curve fits using data from the ICAO databank.

After implementing the fuel flow rate function in FAST, two aircraft with different engines (an ERJ175LR with the CF34-8E5 engine and an A320neo with the LEAP1A26 engine) were selected to examine whether the function accurately estimates the fuel consumption for their respective design missions in FAST. Table 4 lists the differences between the estimated results in FAST and those found in literature, including MTOW, OEW, block fuel and the TSFC in cruise. All the differences are less than 2% by tuning the fuel flow rate, airframe weight, and the lift-drag ratio in climb/cruise. Therefore, these results demonstrated the turbofan off-design engine modeling in FAST has the capability to accurately estimate the performance of sized aircraft.

VII. Case Study: A Notional Electrified Freighter Aircraft

To illustrate FAST's ability to rapidly explore the design space and perform high-level trade studies, a demonstration with a notional model of Lockheed Martin's LM100J (depicted in Fig. 15), a commercial freighter aircraft, using

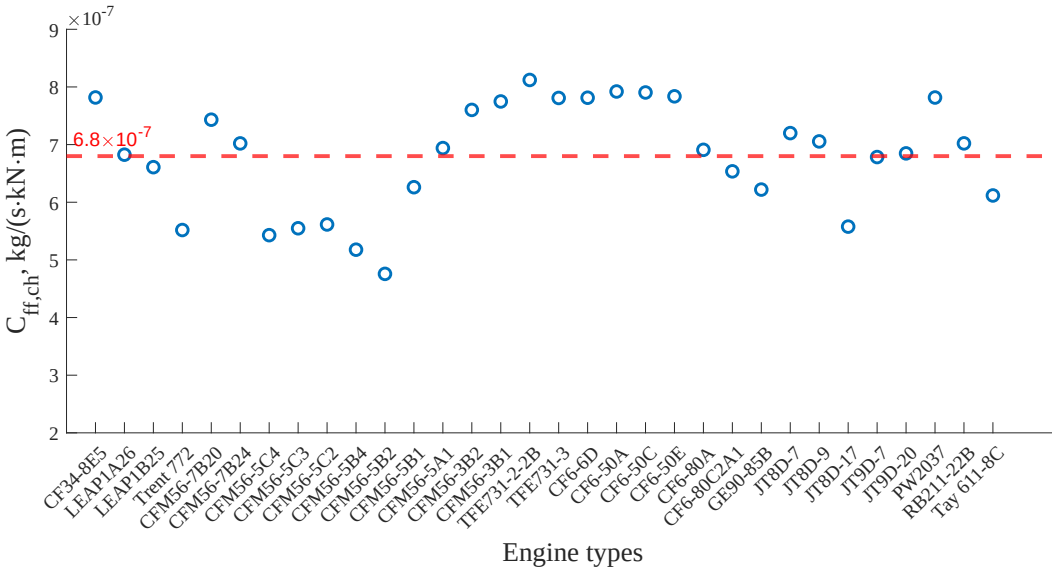

Fig. 14 Simplified linear correlation factor values, $C_{ff,ch}$, for various turbofan engines.

Table 4 Validating the sized aircraft models using FAST's off-design engine modeling capability

Parameter	**ERJ175LR**			**A320neo (Weight Variant 054)**		
(Units)	FAST	Literature	Difference	FAST	Literature	Difference
MTOW (kg)	38,637	38,790 [39]	-0.39%	79,333	79,000 [40, 41]	+0.42%
OEW (kg)	21,545	21,500 [39]	+0.21%	44,581	44,300 [40, 41]	+0.63%
Block fuel (kg)	9,397	9,428 [39]	-0.33%	18,856	18,729**	+0.68%
TSFC in Cruise (lb/lbf/hr)	0.692	0.680 [37]	+1.76%	0.514	0.51 [38]	+0.78%

**Values range from 18,729 to 21,005 kg depending on number of fuel tanks installed, passenger capacity, weight variant, etc. [42]. In this case, the FAST inputs for this design point reflect an A320neo without the additional center fuel tank.

publicly available data. This aircraft is worthy of electrifying because it can carry a 40,000 lbm payload [43]. By replacing part of the payload can be replaced with a battery to electrify the propulsion system, fuel can be saved while still carrying a significant amount of cargo. Furthermore, a similar aircraft was used in previous work by the EPFD team [44]. After discussion with the EPFD team, they were interested in understanding which combinations of design ranges and payloads, electrification technology capabilities, and power management strategies help reduce the aircraft's fuel burn.

The research question posed by the EPFD team was: for an independent parallel hybrid electric aircraft, what are the sensitivities of the block fuel required to fly the mission with respect to the battery specific energy and the percentage of payload removed from the aircraft? In order to answer this question, two aircraft models were made: (1) a conventional notional commercial freighter with four gas-turbine engines, which served as a baseline; and (2) an independent parallel hybrid electric aircraft based on the conventional model, but with the two outboard engines powered by electric motors (as done by Pham et al. [44, 45]). The electrified propulsion architecture is depicted in Fig. 16. Each outboard propeller is connected to its own electric motor. For simplicity, it was assumed that one battery provides the power required to operate both electric motors. The thrust is split amongst the outboard and inboard propellers based on the expressions above each green arrow in Fig. 16. The parameter, λ, is the thrust split, which is defined in Eq. 42 as the fraction of total thrust provided by the outboard (electrified) propellers.

$$\lambda \equiv \frac{\text{Total Thrust Provided by the Outboard Propellers}}{\text{Total Thrust Required}} \tag{42}$$

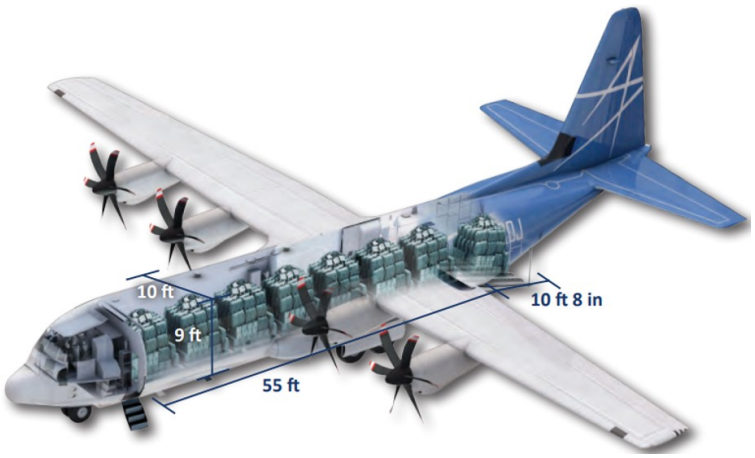

Fig. 15 LM100J freighter aircraft [43]

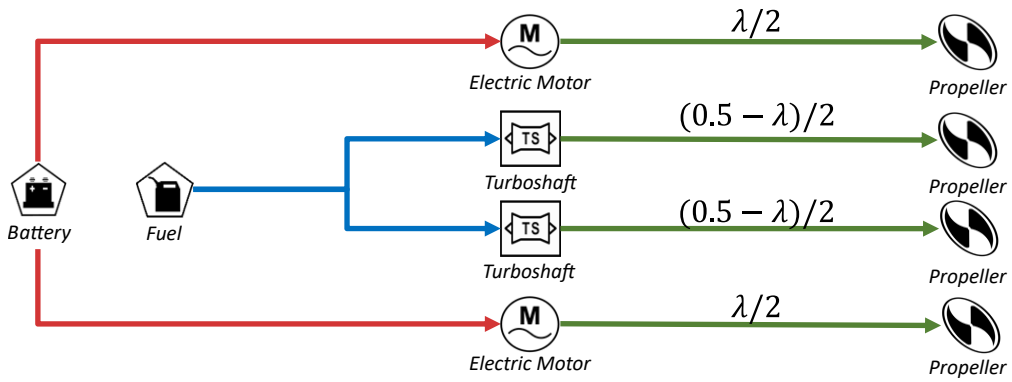

Fig. 16 Electrified propulsion architecture for the LM100J

A. Conventional Freighter Modeling

First, a conventional freighter model was developed and calibrated in FAST. Information from the Federal Aviation Administration's TCDS [46] and Lockheed Martin's informational pamphlet [43] was used to estimate the performance parameters for the commercial freighter, as shown in Tab. 5. The freighter's design mission was prescribed from the EPFD team and consisted of a 2,390 nmi mission, cruising at 25,000 ft and at a speed of Mach 0.59. To properly estimate the block fuel, a 45-minute loiter was added to the design mission and involved flying at 10,000 ft and at a speed of 300 KTAS.

Using the aforementioned aircraft specifications and mission profile, the conventional freighter model was calibrated to match the MTOW, OEW, and block fuel given in by Lockheed Martin for the LM100J [43]. The calibration involved adjusting the cruise and climb/descent lift-drag ratios as well as the turboshaft engine's polytropic efficiencies and total burner temperature. Table 6 contains the values of all these parameters.

The corresponding weights from the calibrated freighter model are provided in Tab. 7. Overall, the calibrated model closely represents the actual MTOW, OEW, and block fuel of the LM100J. Since this study assessed ways to reduce the freighter's fuel burn, the parameters were tuned to most closely match the block fuel value found in literature.

B. System-Level Assessments

Using the conventional freighter model as a baseline, its propulsion system can be electrified, as shown in Fig. 16. This involves powering the outboard propellers by electric motors with a power-weight ratio of 10 kW/kg, and is similar

Table 5 LM100J aircraft specification and performance parameter estimates

Parameter	Units	Value
Design Range	nmi	2,390
Payload	lbm	40,000
Power-Weight Ratio	W/kg	183.4
Wing Loading	lbm/ft^2	123.7
MTOW	lbm	164,000
OEW	lbm	80,350
Block Fuel	lbm	38,000
Cruise Speed	Mach	0.59

Table 6 Parameters tuned to calibrate the conventional freighter model

Parameter	Value
Airframe Weight Scale Factor	0.991
Engine Fuel Flow Scale Factor	1.037
Cruise L/D	14.850
Climb/Descent L/D	12.850
Total Burner Temperature (K)	1,200
Inlet Polytropic Efficiency	0.990
Diffuser Polytropic Efficiency	0.990
Compressor Polytropic Efficiency	0.860
Combustor Polytropic Efficiency	0.980
Turbine Polytropic Efficiency	0.860
Nozzle Polytropic Efficiency	0.985

Table 7 Comparison between the calibrated LM100J and the literature

Weight	Calibrated LM100J	Literature	Percent Error
MTOW (lbm)	159,953	164,000	-2.470%
OEW (lbm)	80,333	80,350	-0.021%
Block Fuel (lbm)	38,001	38,000	+0.003%

to the power-weight ratio of 9.85 kW/kg used previously [44]. The inboard propellers are still powered by turboshaft engines. The calibration factors from Tab. 6 remain constant for all system-level assessments to understand the impacts of new technologies and operational strategies.

The electrified freighter model was first used to perform a retrofit study, which involved removing part of the payload to accommodate the electric motors and battery added to the freighter's propulsion system. After allocating the initial space for the electrified propulsion system, an iteration occurs to find the fuel and battery weights required to fly the mission. This iteration involves flying the design mission to determine the requisite fuel weight and then allocating any remaining weight to the battery such that the electrified freighter's takeoff gross weight (TOGW) matches its MTOW. While flying the design mission, the battery is used for as long as possible until it is fully depleted. Once the battery is fully depleted, the outboard propulsors are turned off and the electrified freighter is only powered by the inboard propulsors. In the EPFD team's previous work [44], the same payload was carried and the electrified freighter's

design range was modified to accommodate the fact that less fuel was carried onboard. Additionally, the EPFD team recommended that improvements to the electrified freighter's performance can be attained by: (1) improving the battery specific energy; (2) off-loading payload; and (3) reducing power demand for the electrified portion of the powertrain.

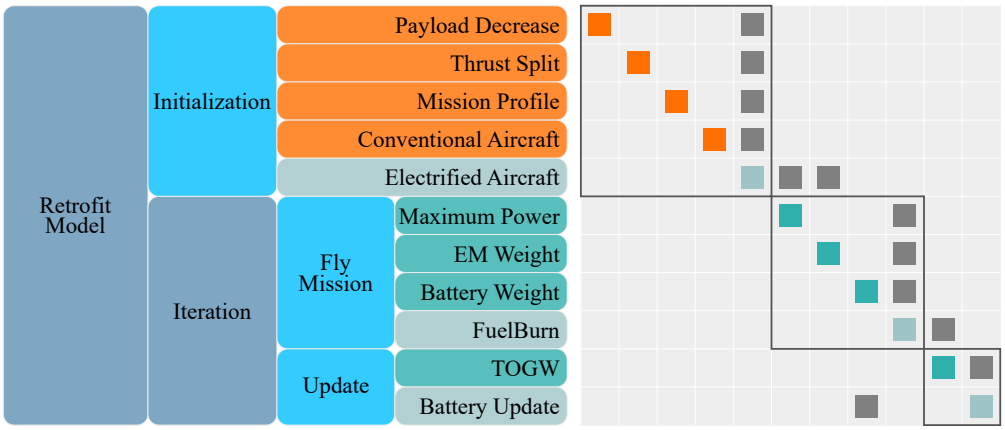

Fig. 17 Computational procedure for retrofitting an aircraft in FAST

The trade studies in this work complement the EPFD team's prior research [44, 45] by fixing the design range and MTOW while varying the battery specific energy, power management strategy (thrust split), and payload carried, thus addressing the areas of improvement that they identified. Table 8 lists the three design variables, along with their upper and lower bounds. The thrust split is treated as a discrete variable, and is sampled in 10% increments. The payload removed and battery specific energy are treated as continuous variables. In this study, the aircraft is assumed to fly with a constant thrust split until the battery runs out of energy – no time- or segment-dependent power management strategies are implemented.

Table 8 Design space for retrofit study

Parameter	Units	Lower Bound	Upper Bound
Payload Removed	%	0	100
Thrust Split	%	10	30
Battery Specific Energy	kWh/kg	0.35	1.55

The electrified freighter's fuel burn will be compared to that of two different baseline aircraft. The first comparison is between a conventional freighter with the same TOGW as the electrified one. Since the conventional aircraft doesn't have to accommodate the battery and electric motor, it will carry more payload than the electrified one. Comparing these two aircraft answers the question: "How much fuel can be saved if payload is sacrificed for an electrified propulsion system?" The second comparison is between a conventional freighter flying at a smaller TOGW, but carrying the same payload as the electrified one. Since the electrified freighter must carry a battery and electric motors, this study quantifies the impacts of the weight penalty associated with electrifying the aircraft's propulsion system and answers the question: "Are the fuel savings from the electrified aircraft better than simply reducing the payload carried by the conventional aircraft?" A notional weight breakdown of each comparison aircraft is shown in Fig. 18. The left bar represents the conventional aircraft flying at the same TOGW as the electrified aircraft. The center bar represents the conventional aircraft carrying the same payload as the electrified aircraft, but flying at a smaller TOGW. The right bar represents the electrified aircraft.

The results presented in this section involve treating the battery specific energy and payload removed as continuous variables and the thrust split as a discrete variable. It was previously mentioned that the electrified aircraft flies with a constant thrust split until the battery runs out of energy. The following figures contain results from the retrofit study. In these figures, the left plot represents the block fuel change between the conventional and electrified aircraft flying at the same MTOW (the left and right bars in Fig. 18). The right plot represents the block fuel change between the

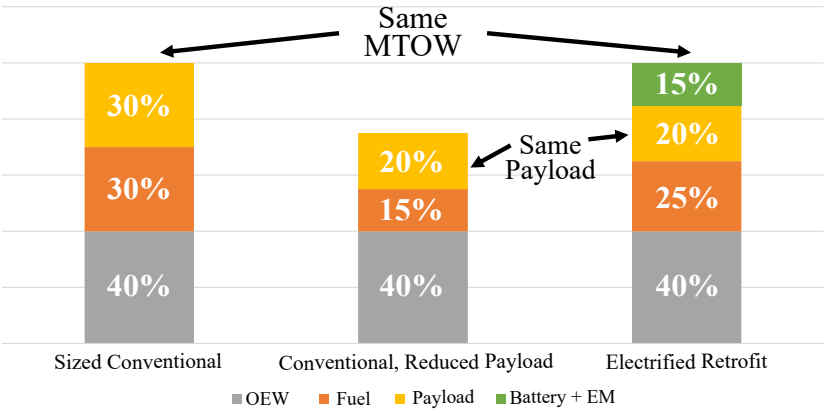

Fig. 18 Notional weight breakdown of aircraft compared in the retrofit study

conventional and electrified aircraft carrying the same payload (the center and right bars in Fig. 18). Note that the lift-drag ratio difference between carrying a full or partial payload is not accounted for – it is assumed that both aircraft fly at the same lift-drag ratios during the different flight phases. Also, the bounds of the horizontal and vertical axes represent the bounds of battery specific energy and payload removed, respectively, provided in Tab. 8.

Figure 19 shows contours of the block fuel change between the conventional and electrified freighter for a 10% thrust split. In the left plot (comparing aircraft of the same MTOW), it was found that electrifying the aircraft at the same MTOW always saves fuel. For small percentages of payload removed from the electrified freighter, a 1 to 5% fuel savings can be achieved, regardless of the battery specific energy available. If larger percentages of the payload are removed, then a greater fuel savings (between 5 to 9%) can be achieved. However, this is not desirable because the electrified freighter is carrying much less payload than its conventional counterpart. Observe that the contours of constant fuel burn change are steeper for lower battery specific energies. This suggests that improving the battery technology will have a greater impact on the fuel burn savings than removing payload from the aircraft. Conversely, once the battery technology matures (and grows to be between 1.0 and 1.5 kWh/kg), the contours of constant fuel burn change a not as steep. Then, it would be more beneficial to remove payload from the aircraft instead of improving the battery technology.

In the right plot (comparing aircraft carrying the same payload), it was found that electrifying the aircraft and carrying the same payload requires more fuel to be burned for most configurations. This is due to the weight penalty from electrifying the propulsion system – the battery and electric motors increase the aircraft's TOGW. There are some combinations of battery specific energy and payload decrease in the lower right-hand corner of the plot that do exhibit a fuel savings. However, this is for higher battery specific energy values that have not yet been attained. Despite the weight penalty imposed by the electrified system, an interesting behavior emerges. At some point, the contours of constant block fuel change become horizontal, and are marked with the white dashed line. The horizontal lines indicate that the block fuel required to fly the mission is constant, regardless of the battery technology available. This suggests that the thrust split is too low and not all of the battery's available energy is being used. Otherwise, the block fuel change would improve for larger battery specific energy values. In other words, part of the battery carried by the electrified aircraft is "dead weight", and is not being used to fly the mission. In order to fully reap the benefits of electrifying the propulsion system, the aircraft should be operated at a higher thrust split.

Figure 20 shows contours of the block fuel change between the conventional and electrified freighter for a 20% thrust split. In the left plot (comparing aircraft of the same MTOW), fuel is saved by increasing the battery specific energy and removing payload. However, there are now some cases with no fuel burn savings, particularly in the lower left-hand corner of the plot. Since the electric motors doubled in size (relative to the ones used for a 10% thrust split), the battery became smaller to accommodate the larger electric motors and ensure that the electrified aircraft did not exceed MTOW. Therefore, the battery supplied energy to the electrified aircraft for a much shorter period of time, and more fuel needed to be carried to fly the mission. Similar to the results for a 10% thrust split, the contours of constant block fuel change are steeper for smaller battery specific energy values. The contours of constant block fuel change are not as steep for larger battery specific energy values. Again, this implies that the best way to save fuel is by improving

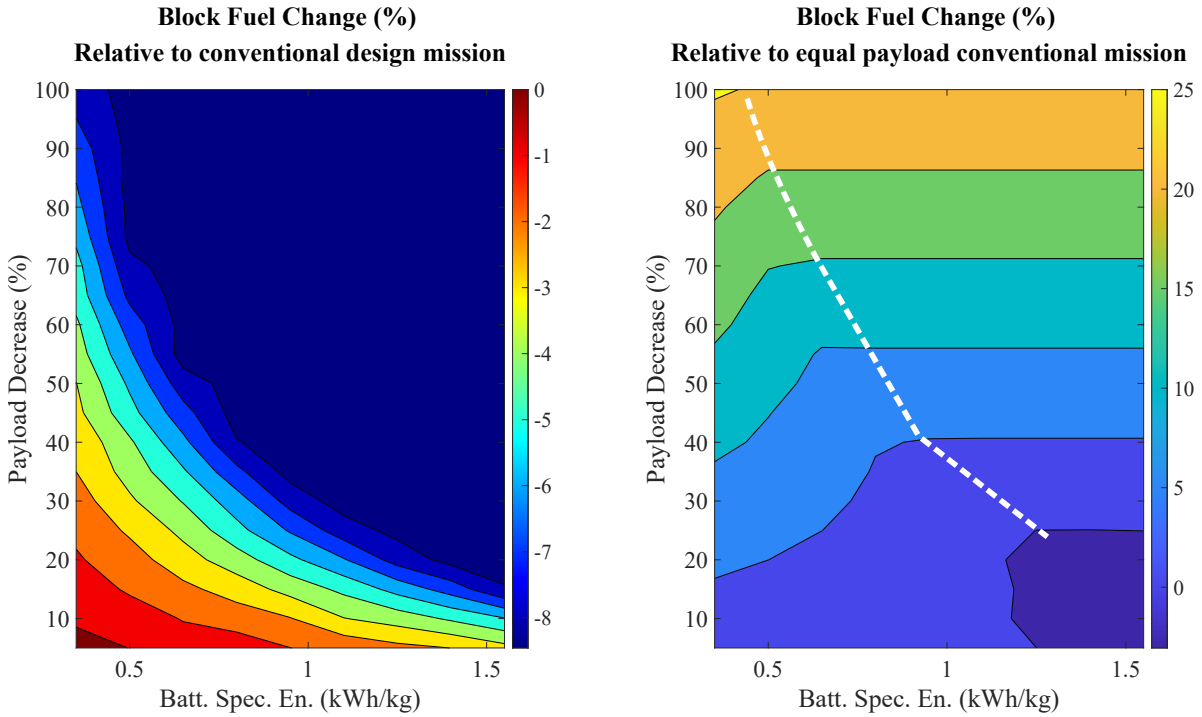

Fig. 19 Block fuel change for an electrified freighter operating at a 10% thrust split relative to the conventional freighter with the same TOGW (left) and payload (right)

the battery technology rather than removing payload from the aircraft.

In the right plot (comparing aircraft carrying the same payload), a similar behavior emerges as was shown while operating the electrified freighter at a 10% thrust split. More fuel was required for most of the missions due to the weight penalty associated with electrifying the propulsion system. Lines of constant block fuel change are still horizontal for larger battery specific energy values, indicating that not all of the battery is used while flying the mission. Towards a battery specific energy of 1.5 kWh/kg, an interesting point emerges, and is denoted with a white dot in Fig. 20. Beyond this point, increasing the battery specific energy allows the designer to add payload back into the aircraft. This is reflected by the contour with a negative slope underneath the point of interest – increasing the battery specific energy and adding payload back into the aircraft burns the same amount of fuel as the white point. Conversely, another part of the contour above the point of interest has a positive slope – increasing the battery specific energy and removing more payload burns the same amount of fuel as the white point. From an operational perspective, this is undesirable because the battery is too heavy and will not be fully used during the mission.

Lastly, Fig. 21 shows contours of the block fuel change between the conventional and electrified freighter for a 30% thrust split. In the left plot (comparing aircraft of the same MTOW), fuel is saved by increasing the battery specific energy and removing payload. Additionally, there are more combinations of payload removed and battery specific energy in the lower left-hand corner that do not exhibit any fuel burn savings. Again, this is due to the fact that the electric motors have tripled in size (relative to the electric motors sized for the 10% thrust split) and the battery must become smaller to ensure that the electrified aircraft doesn't exceed MTOW. Also, the slopes of the contours are similar to the previous cases, but are less steep at lower battery specific energy values. This suggests that, for higher thrust splits, removing payload or improving the battery specific energy has the same impact on the fuel burn savings.

In the right plot (comparing aircraft carrying the same payload), a similar trend emerges – more fuel is required to fly the mission due to the weight penalty imposed by the electrified propulsion system. Lines of constant block fuel change still exist, but only for cases in which nearly all of the payload is removed from the electrified freighter, which does not make sense to pursue from an operational perspective. Again, a critical point emerges (white point) – the contour of constant block fuel change has both a positive slope and negative slope as the battery specific energy increases. As previously mentioned, following the contour with a negative slope is more desirable because payload can be added back

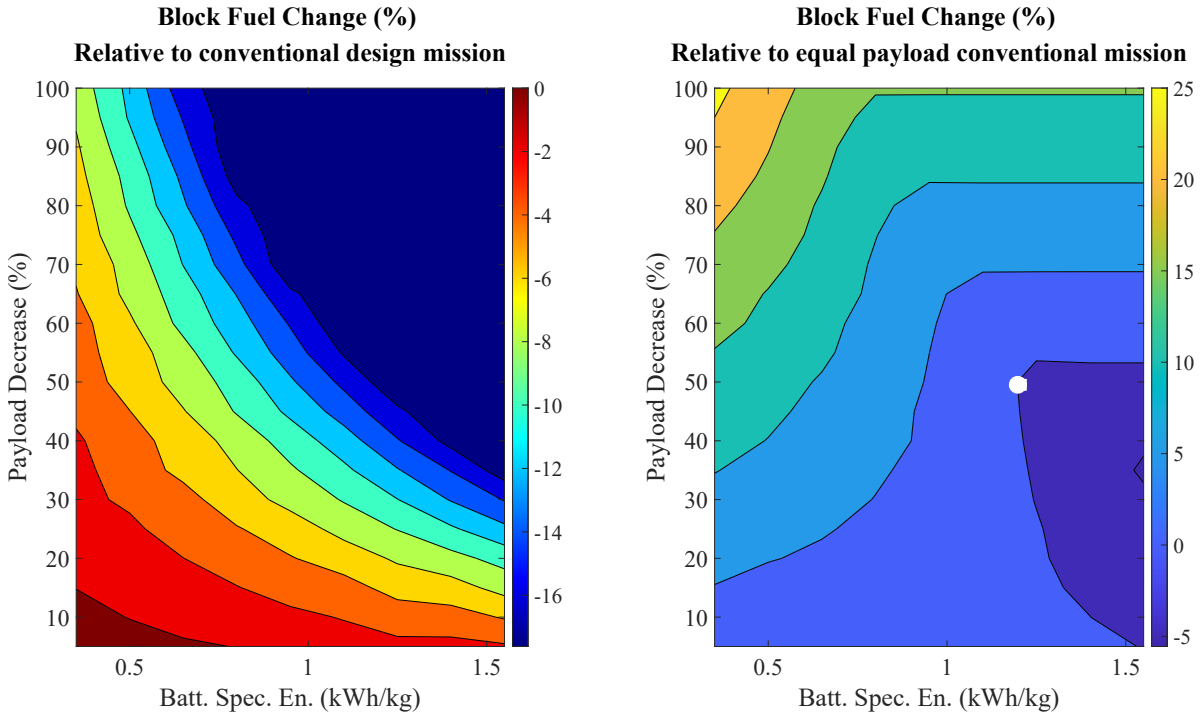

Fig. 20 Block fuel change for an electrified freighter operating at a 20% thrust split relative to the conventional freighter with the same TOGW (left) and payload (right)

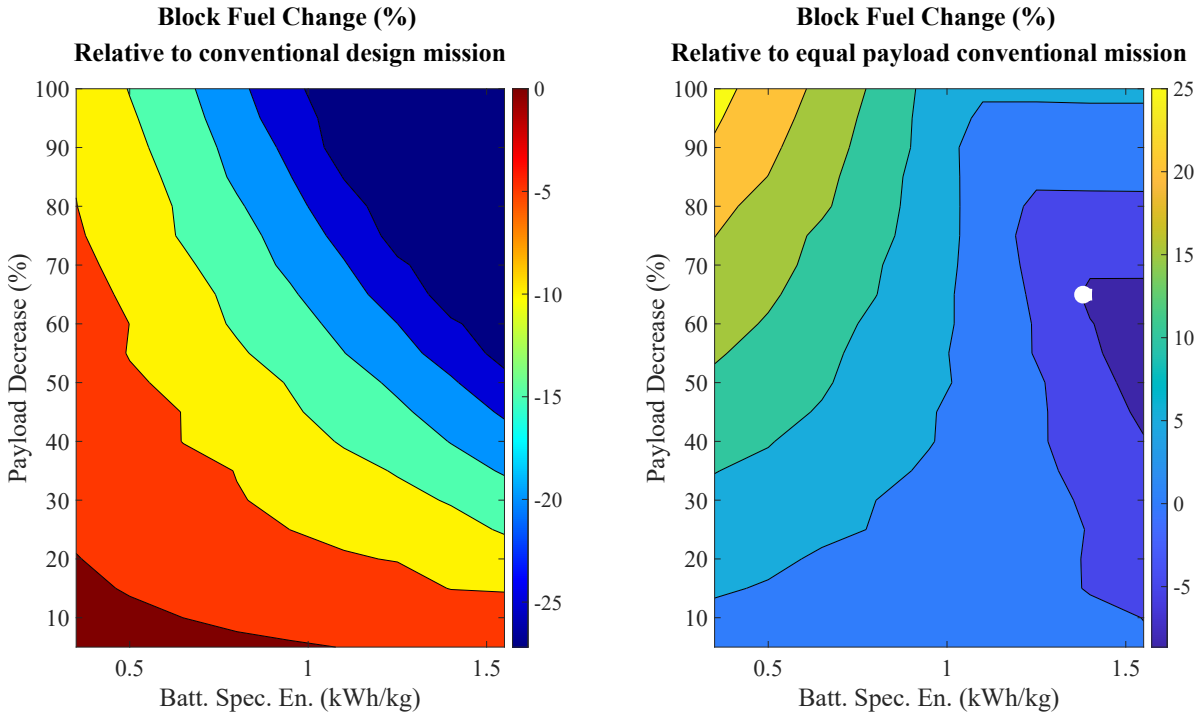

Fig. 21 Block fuel change for an electrified freighter operating at a 30% thrust split relative to the conventional freighter with the same TOGW (left) and payload (right)

into the aircraft as the battery specific energy improves. This makes the electrified freighter a more operationally viable alternative to a conventionally gas-turbine powered freighter jet. Also, towards a battery specific energy of 1.25 kWh/kg, the slope of the contours change from positive to negative. This indicates that there is a critical battery specific energy that will provide the same block fuel change regardless of how much payload is removed. Additional work is needed to quantify this point and further explore its ramifications.

VIII. Conclusions and Future Work

The Future Aircraft Sizing Tool (FAST) presented here provides an advanced, open-source platform for early-phase conceptual design across a range of propulsion architectures, including electrified configurations. FAST distinguishes itself with several novel capabilities:

- **Propulsion-agnostic design flexibility:** FAST accommodates a wide range of propulsion architectures without requiring specific propulsion dependencies, enabling comparative analysis across architectures, such as hybrid-electric, fully electric, and conventional designs.
- **Integrated engine modeling:** Unlike many aircraft sizing tools that rely on external models or engine decks, FAST incorporates a built-in engine model capable of directly sizing and simulating turbofan, turbojet, and turboprop engines without predefined engine performance decks. This feature allows FAST to dynamically evaluate fuel consumption, thrust, and efficiency under varied mission conditions.
- **Rapid, integrated aircraft sizing and performance analysis:** The tool's fast convergence (typically under one minute) facilitates iterative design exploration, even for complex propulsion configurations.
- **Historical aircraft database and data-driven modeling:** Leveraging a dataset of over 450 historical aircraft, FAST integrates data-driven models for accurate initial parameter estimations, which support early-phase design efforts when complete specifications may be unavailable.
- **Energy-based mission analysis:** FAST applies an energy-based mission analysis approach, enabling flexible assessment across diverse mission profiles and making it particularly well-suited for evaluating energy-sensitive configurations like electrified aircraft.

FAST's capabilities make it an effective tool for design space exploration and sensitivity analysis, addressing the current need for flexible, propulsion architecture-independent tools that support emerging technologies in aviation. The source code for FAST is freely available on GitHub[**].

To showcase FAST's capabilities, the case study examined a notional commercial freighter, partially electrified by powering its outboard propellers with electric motors. In both retrofit studies, a portion of the payload was removed to allocate space for the battery, as the added weight of the electrified system increased the aircraft's takeoff gross weight. In the first retrofit study, the electrified freighter's TOGW matched the MTOW of the conventional aircraft. The study's results indicate that improving the battery specific energy has a more significant impact on fuel savings than further payload reduction. Specifically, the battery technology must mature to very high specific energy levels (around 1.0-1.5 kWh/kg) for potential fuel savings to become substantial without additional payload sacrifices. With lower battery-specific energy values (up to 0.60 kWh/kg for a 10% thrust split and 0.75 kWh/kg for a 20% thrust split), payload reductions offer only limited fuel savings. In the second retrofit study, both the conventional and electrified freighters carried the same payload. Due to the weight penalty associated with electrifying the propulsion system, the conventional aircraft had a lower TOGW than the electrified one. To save fuel with this operational strategy, the battery technology must mature to at least 1.0 kWh/kg. For 20% and 30% thrust splits, there exists a critical battery specific energy (at about 1.25 and 1.40 kWh/kg, respectively) in which a fuel savings is attained. Further increasing the battery specific energy beyond this point allows payload to be added back into the aircraft, thus improving its operational viability.

Future improvements to FAST could further expand its analytical robustness and usability. Enhancing the GPMs within FAST to refine historical regressions would boost predictive accuracy across key performance metrics. Secondly, unifying the governing equations for the climb, cruise, and descent segments could simplify mission analysis, streamlining both code maintenance and performance evaluation. Additionally, incorporating analytical differentiation could enable gradient-based optimization, making FAST more adaptable for sensitivity analyses and broader optimization tasks critical to early-phase aircraft design.

[**] https://github.com/ideas-um/FAST

IX. Appendix

Appendices IX.A through IX.D list all of the possible parameters to describe an aircraft design and design mission profile in FAST. Appendix IX.E is a follow-up to the energy-based segment analysis from Section V.A and provides an algorithm for the reader to replicate the analysis by themselves. Appendix IX.F is a follow-up to the off-design gas-turbine engine modeling from Section VI.E and provides the necessary coefficients to estimate the fuel flow to power a turbofan engine.

A. Aircraft Specification Parameters

The Aircraft Specification File was introduced in Section II.A and described the disciplines/groups of parameters that can be provided. The parameters are specified in Matlab as part of a data structure: `Aircraft.Specs.Discipline.Variable.Sub-type`, where `Discipline`, `Variable`, and `Sub-type` are provided in Tab. 9. If a row is *italicized*, it is a required input into FAST; all others are optional. All variables not specified by the user are predicted by either default values or the GPMs introduced in Section III.

Table 9 All variables that can be specified in FAST

Discipline	Variable	Sub-type	Description
TLAR	EIS		Entry-into-Service Year
TLAR	*Class*		*Aircraft Class ("Turbofan", "Turboprop", or "Piston")*
TLAR	*MaxPax*		*Maximum Number of Passengers Carried*
Performance	Vels	Tko	Takeoff Speed [m/s]
Performance	Vels	Crs	Cruise Speed [Mach]
Performance	Alts	Tko	Takeoff Altitude [m]
Performance	Alts	Crs	Cruise Altitude [m]
Performance	RCMax		Maximum Rate-of-Climb [m/s]
Performance	*Range*		*Design Range [m]*
Aero	L_D	Clb	Climb Lift-Drag Ratio
Aero	L_D	Crs	Cruise Lift-Drag Ratio
Aero	L_D	Des	Descent Lift-Drag Ratio
Aero	W_S	SLS	Wing Loading [kg/m^2]
Weight	MTOW		Maximum Takeoff Weight [kg]
Weight	EG		Electric Generator Weight [kg]
Weight	EM		Electric Motor Weight [kg]
Weight	Fuel		Fuel Weight [kg]
Weight	Batt		Battery Weight [kg]
Weight	WairCF		Airframe Weight Calibration Factor
Propulsion	Engine		Function Handle to Engine Model
Propulsion	NumEngines		Number of Engines Installed
Propulsion	T_W	SLS	Sea-Level Static Thrust-Weight Ratio (turbofan only)
Propulsion	Thrust	SLS	Sea-Level Static Thrust Produced by Aircraft [N]
Propulsion	MDotCF		Fuel Flow Calibration Factor
Propulsion	*Arch*	*Type*	*Propulsion Architecture*
Power	SpecEnergy	Fuel	Fuel Gravimetric Specific Energy [kWh/kg]
Power	SpecEnergy	Batt	Battery Gravimetric Specific Energy [kWh/kg]
Power	Eta	EM	Electric Motor Efficiency [%]

Table 9 All variables that can be specified in FAST

Discipline	Variable	Sub-type	Description
Power	Eta	EG	Electric Generator Efficiency [%]
Power	Eta	Propeller	Propeller Efficiency [%]
Power	P_W	SLS	Aircraft Power-Weight Ratio (turboprop/piston only) [kW/kg]
Power	P_W	EM	Electric Motor Power-Weight Ratio
Power	P_W	EG	Electric Generator Power-Weight Ratio
Power	LamTS	Tko	Takeoff Thrust Split [%]
Power	LamTS	Clb	Climb Thrust Split [%]
Power	LamTS	Crs	Cruise Thrust Split [%]
Power	LamTS	Des	Descent Thrust Split [%]
Power	LamTS	Lnd	Landing Thrust Split [%]
Power	LamTS	SLS	Design Thrust Split [%]
Power	LamTSPS	Tko	Takeoff Thrust-Power Source Split [%]
Power	LamTSPS	Clb	Climb Thrust-Power Source Split [%]
Power	LamTSPS	Crs	Cruise Thrust-Power Source Split [%]
Power	LamTSPS	Des	Descent Thrust-Power Source Split [%]
Power	LamTSPS	Lnd	Landing Thrust-Power Source Split [%]
Power	LamTSPS	SLS	Design Thrust-Power Source Split [%]
Power	LamPSPS	Tko	Takeoff Power-Power Source Split [%]
Power	LamPSPS	Clb	Climb Power-Power Source Split [%]
Power	LamPSPS	Crs	Cruise Power-Power Source Split [%]
Power	LamPSPS	Des	Descent Power-Power Source Split [%]
Power	LamPSPS	Lnd	Landing Power-Power Source Split [%]
Power	LamPSPS	SLS	Design Power-Power Source Split [%]
Power	LamPSES	Tko	Takeoff Power-Energy Source Split [%]
Power	LamPSES	Clb	Climb Power-Energy Source Split [%]
Power	LamPSES	Crs	Cruise Power-Energy Source Split [%]
Power	LamPSES	Des	Descent Power-Energy Source Split [%]
Power	LamPSES	Lnd	Landing Power-Energy Source Split [%]
Power	LamPSES	SLS	Design Power-Energy Source Split [%]
Power	Battery	ParCells	Battery Cells in Parallel
Power	Battery	SerCells	Battery Cells in Series
Power	Battery	BegSOC	Initial Battery SOC [%]

B. Engine Specification Parameters

The engine specification file was introduced in Section VI and described the disciplines/groups of parameters that can be provided. The parameters are specified in Matlab as part of a data structure: `Engine.Variable.Sub-type`, where `Variable`, and `Sub-type` are provided from Tab. 10. The “Engine Type" column shows whether a variable is relevant to turbofan engines or turboprop engines, denoted by flags “F" and “P," respectively. All variables must be specified in an input function to successfully size an engine, however in the case that an aircraft specification file does not reference an engine function handle, one is created using default values or the GPMs introduced in Section III.

Table 10 Engine variables that are specified in FAST

Engine Type	Variable	Sub-type	Description
F & P	Mach		Free stream Mach number
F & P	Alt		Free stream altitude [m]
F & P	OPR		Ratio of post high-pressure-compressor air pressure to ambient air pressure
F & P	BPR		Bypass ratio
F & P	Tt4Max		Maximum Combustion Chamber Temperature [K]
F	DesignThrust		Desired thrust output [N]
P	ReqPower		Desired power output [W]
F & P	NoSpools		Number of shafts in the engine
F & P	RPMs		Vector of length NoSpools giving shaft speeds [RPM]
F	FanGearRatio		Fan speed to low-pressure-turbine speed ratio
F	FanBoosters		Boolean flag denoting additional compressor stages coupled to fan shaft
F & P	CoreFlow	PaxBleed	Percentage of core airflow used for passenger bleed air[%]
F & P	CoreFlow	Leakage	Percentage of core airflow assumed to leak [%]
F & P	CoreFlow	Cooling	Percentage of core airflow used for turbine cooling [%]
F	EtaPoly	Inlet	Polytropic inlet efficiency
F & P	EtaPoly	Diffusers	Polytropic diffuser efficiency
F	EtaPoly	Fan	Polytropic fan efficiency
F & P	EtaPoly	Compressors	Polytropic compressor efficiency
F & P	EtaPoly	Combustor	Polytropic combustor efficiency
F & P	EtaPoly	Turbines	Polytropic turbine efficiency
F & P	EtaPoly	Nozzles	Polytropic nozzle efficiency
F & P	MaxIter		Maximum iterations allotted for engine design convergence
F & P	Visualize		Flag denoting if the engine should be visualized after sizing is complete

C. Run Settings

In addition to the parameters specified in Appendix IX.D, the Aircraft Specification File can also contain a variety of Run Settings that can be used to make the aircraft analysis more/less detailed. These settings are provided in Tab. IX.C, and are all optional inputs.

Table 11 All run settings that can be specified in FAST

Setting	Sub-Setting	Description
TkoPoints		Number of Control Points in a Takeoff Segment
ClbPoints		Number of Control Points in a Climb Segment
CrsPoints		Number of Control Points in a Cruise Segment
DesPoints		Number of Control Points in a Descent Segment
OEW	MaxIter	Maximum Number of OEW Estimation Iterations
OEW	Tol	Convergence Tolerance for OEW Estimation
Analysis	MaxIter	Maximum Number of Aircraft Sizing/Performance Iterations
Analysis	Tol	Convergence Tolerance for Aircraft Sizing/Performance
Plotting		Mission History Plotting Flag
Table		Tabulate Mission History Flag
VisualizeAircraft		Aircraft Visualization Flag
Dir	Size	Directory of FAST
Dir	Oper	Alternate Working Directory (outside of FAST)

D. Mission Profile Parameters

The Mission Profile Specification File was introduced in Section II.B and illustrated an example of a mission profile. The parameters required to define a mission profile are provided in Tab. 12. All parameters are required, except for `ClbRate`, which can be input as either a value or `NaN` for climb, cruise, and descent semgents, and `NaN` for takeoff and landing segments.

Table 12 Parameters to define the mission profile

Variable	Type	Description
Segs		Segments to be flown in the mission profile
Target	Type	Specifies whether a distance- or time-based target is flown
Target	Valu	Distance/Time specified by the mission target type
ID		Number to connect a mission segment to a mission target
AltBeg		Beginning altitude [m]
AltEnd		Ending altitude [m]
VelBeg		Beginning airspeed [m/s or Mach]
VelEnd		Ending airspeed [m/s or Mach]
TypeBeg		Beginning airspeed type [“TAS”, “EAS”, or “Mach”]
TypeEnd		Ending airspeed type [“TAS”, “EAS”, or “Mach”]
ClbRate		Climb/Descent Rate [m/s or NaN]

E. Energy-Based Segment Analysis Algorithm

The algorithm used to perform the energy-based segment analysis in Section V.A is provided in Algorithm 1.

Algorithm 1 Energy-based mission analysis

Input $h^{(1)}$, $V_\infty^{(1)}$, $h^{(n)}$, and $V_\infty^{(n)}$
Initialize altitudes at control points by linearly interpolating between $h^{(1)}$ and $h^{(n)}$
Initialize airspeeds at control points by linearly interpolating between $V_\infty^{(1)}$ and $V_\infty^{(n)}$
Compute the energy heights using Eq. 13
if aircraft is a turbofan **then**
    Compute TV_∞ using Eq. 14
else
    Compute TV_∞ using Eq. 15
end if
Predict the lift using Eq. 16
Predict the drag using Eq. 17
Compute the specific excess power using Eq. 18
if rate of climb is provided **then**
    Compute Δt using Eq. 19
    Compute the maximum realizable acceleration using Eq. 20
    if any $\frac{dV_\infty}{dt} > \left(\frac{dV_\infty}{dt}\right)_{\max}$ **then**
        Set $\frac{dV_\infty}{dt} = \left(\frac{dV_\infty}{dt}\right)_{\max}$ where applicable
        Re-compute the airspeed profile: $V_\infty^{(i)} = V_\infty^{(i-1)} + \left(\frac{dV_\infty}{dt}\right)^{(i-1)} \Delta t^{(i-1)}$
    end if
else
    Compute Δt using Eq. 21
    if any $\frac{dh}{dt} > \left(\frac{dh}{dt}\right)_{\max}$ **then**
        Set $\frac{dh}{dt} = \left(\frac{dh}{dt}\right)_{\max}$ where applicable
        Re-compute Δt using Eq. 19
    end if
end if
Compute $\frac{dh}{dt}$ using Eq. 22
Compute $\frac{dV_\infty}{dt}$ using Eq. 23
Compute the aircraft-level power required using Eq. 24
Propagate the aircraft-level power required to the components in the propulsion system
Compute the energy required by each energy source using Eq. 25

F. Off-design turbofan engine modeling coefficients

In Section VI.E, Eqs. 39 through 41 explained how to compute the fuel flow in a turbofan engine using data from the *ICAO Aircraft Emissions Databank* [35]. Table 13 lists the required coefficients to estimate the fuel flow for a variety of turbofan engines.

Table 13 Off-design turbofan engine modeling coefficients and cruise TSFC

Engine	$C_{ff,3}\left(\frac{kg}{s}\right)$	$C_{ff,2}\left(\frac{kg}{s}\right)$	$C_{ff,1},\left(\frac{kg}{s}\right)$	$C_{ff,ch}\left(\frac{kg}{kN\times s\times m}\right)$	$TSFC_{Cr}\left(\frac{kg}{kN\times s}\right)$
CF34-8E5	0.2992	−0.3464	0.7012	7.8175×10^{-7}	1.93×10^{-2}
LEAP1A26	0.3940	−0.4938	0.9638	6.8249×10^{-7}	1.44×10^{-2}
LEAP1B25	0.4033	−0.4374	0.9833	6.6083×10^{-7}	1.50×10^{-2}
Trent 772	1.5189	−1.5650	3.2532	5.5180×10^{-7}	1.60×10^{-2}
CFM56-7B20	0.4248	−0.6031	1.0944	7.4318×10^{-7}	1.79×10^{-2}
CFM56-7B24	0.4708	−0.5909	1.2262	7.0206×10^{-7}	1.78×10^{-2}
CFM56-5C4	0.3928	−0.3230	1.3895	5.4289×10^{-7}	1.54×10^{-2}
CFM56-5C3	0.3720	−0.3372	1.3415	5.5485×10^{-7}	1.54×10^{-2}
CFM56-5C2	0.4172	−0.4225	1.3165	5.6145×10^{-7}	1.54×10^{-2}
CFM56-5B4	0.4107	−0.4658	1.2238	5.1770×10^{-7}	1.54×10^{-2}
CFM56-5B2	0.5168	−0.4719	1.3839	4.7575×10^{-7}	1.54×10^{-2}
CFM56-5B1	0.4273	−0.3966	1.3314	6.2608×10^{-7}	1.69×10^{-2}
CFM56-5A1	0.4370	−0.5006	1.1176	6.9397×10^{-7}	1.69×10^{-2}
CFM56-3B2	0.5239	−0.7323	1.2685	7.6016×10^{-7}	1.89×10^{-2}
CFM56-3B1	0.4970	−0.7408	1.1938	7.7482×10^{-7}	1.89×10^{-2}
TFE731-2-2B	0.1099	−0.1797	0.2755	8.1211×10^{-7}	2.31×10^{-2}
TFE731-3	0.1594	−0.2396	0.3059	7.8088×10^{-7}	2.32×10^{-2}
CF6-6D	0.6881	−0.8084	1.8619	7.8130×10^{-7}	1.83×10^{-2}
CF6-50A	0.6427	−0.7307	2.2570	7.9211×10^{-7}	1.85×10^{-2}
CF6-50C	0.5913	−0.5759	2.2664	7.9039×10^{-7}	1.86×10^{-2}
CF6-50E	0.5826	−0.5468	2.3256	7.8372×10^{-7}	1.86×10^{-2}
CF6-80A	0.1966	−0.1296	2.0786	6.9091×10^{-7}	1.76×10^{-2}
CF6-80C2A1	0.8280	−0.7522	2.3288	6.5360×10^{-7}	1.63×10^{-2}
GE90-85B	1.3008	−1.3348	3.2336	6.2196×10^{-7}	1.47×10^{-2}
JT8D-7	0.7009	−0.9494	1.2431	7.1991×10^{-7}	2.25×10^{-2}
JT8D-9	0.7856	−1.0425	1.3023	7.0552×10^{-7}	2.27×10^{-2}
JT8D-17	1.0575	−1.3668	1.5596	5.5773×10^{-7}	2.27×10^{-2}
JT9D-7	0.4007	−0.5522	2.2412	6.7839×10^{-7}	1.76×10^{-2}
JT9D-20	0.2833	−0.4244	2.2468	6.8476×10^{-7}	1.77×10^{-2}
PW2037	0.3800	−0.2765	1.4395	7.8166×10^{-7}	1.65×10^{-2}
RB211-22B	1.4623	−2.0834	2.5004	7.0212×10^{-7}	1.78×10^{-2}
Tay 611-8C	0.6785	−1.0341	1.1006	6.1175×10^{-7}	2.01×10^{-2}

Funding Sources

This work is sponsored by the NASA Aeronautics Research Mission Directorate and Electrified Powertrain Flight Demonstration project, "Development of a Parametrically Driven Electrified Aircraft Design and Optimization Tool", Glenn Engineering and Research Support Contract (GEARS) Contract No. 80GRC020D0003.

Acknowledgments

The authors would like to thank Ralph Jansen, Amy Chicatelli, Andrew Meade, Karin Bozak, Noah Listgarten, Dennis Rohn, and Gaudy Bezos-O'Connor from NASA's Electrified Powertrain Flight Demonstration project for supporting this work and providing valuable technical input and feedback throughout the duration of the project. The authors also thank Huseyin Acar, Rawan Aljaber, Swapnil Jagtap, Nawa Khailany, Janki Patel, Joaquin Rey, Jayda Shine, and Michael Tsai for their contributions to either FAST or the historical aircraft database that the regressions and projections rely on.

References

[1] Jansen, R., Brown, G. V., Felder, J. L., and Duffy, K. P., "Turboelectric aircraft drive key performance parameters and functional requirements," *51st AIAA/SAE/ASEE joint propulsion conference*, 2015, p. 3890.

[2] National Aeronautics, and Space Administration, "Electrified Aircraft Propulsion (EAP)," https://www1.grc.nasa.gov/aeronautics/eap/, 2024.

[3] National Aeronautics, and Space Administration, "About Electrified Powertrain Flight Demonstration Project," https://www.nasa.gov/directorates/armd/integrated-aviation-systems-program/armd-iasp-epfd/about-electrified-powertrain-flight-demonstration-project/, 2022.

[4] National Aeronautics and Space Administration, "Subsonic Single Aft Engine (SUSAN) Aircraft," https://www1.grc.nasa.gov/aeronautics/eap/airplane-concepts/susan/, 2023.

[5] National Aeronautics and Space Administration, "Single-Aisle Turboelectric Aircraft with Aft Boundary Layer Propulsion (STARC-ABL)," https://www1.grc.nasa.gov/aeronautics/eap/airplane-concepts/starc-abl/, 2023.

[6] Cinar, G., Cai, Y., Denney, R. K., and Mavris, D. N., "Modeling and Simulation of a Parallel Hybrid Electric Regional Aircraft for the Electrified Powertrain Flight Demonstration (EPFD) Program," *2022 IEEE Transportation Electrification Conference & Expo (ITEC)*, IEEE, 2022, pp. 670–675.

[7] Cinar, G., Cai, Y., Bendarkar, M. V., Burrell, A. I., Denney, R. K., and Mavris, D. N., "System analysis and design space exploration of regional aircraft with electrified powertrains," *Journal of Aircraft*, Vol. 60, No. 2, 2023, pp. 382–409.

[8] Lents, C. E., Hardin, L. W., Rheaume, J., and Kohlman, L., "Parallel hybrid gas-electric geared turbofan engine conceptual design and benefits analysis," *52nd AIAA/SAE/ASEE joint propulsion conference*, 2016, p. 4610.

[9] Chau, T., Kenway, G., and Kiris, C. C., "Conceptual Exploration of Aircraft Configurations for the SUSAN Electrofan," *AIAA SciTech 2022 Forum*, 2022, p. 2181.

[10] Chau, T., and Duensing, J., "Conceptual Design of the Hybrid-Electric Subsonic Single Aft Engine (SUSAN) Electrofan Transport Aircraft," *AIAA SCITECH 2024 Forum*, 2024, p. 1326.

[11] Haglage, J., Dever, T., Jansen, R., and Lewis, M., "Electrical System Trade Study for SUSAN Electrofan Concept Vehicle," *AIAA SciTech 2022 Forum*, 2022, p. 2183.

[12] Cai, Y., Xie, J., Cinar, G., and Mavris, D. N., "Advanced 2030 turboprop aircraft modeling for the electrified powertrain flight demonstration program," *2022 IEEE Transportation Electrification Conference & Expo (ITEC)*, IEEE, 2022, pp. 664–669.

[13] Recine, C., Pham, D., Bowles, J., Lyons, K., Margolis, B., and Garcia, J. A., "Analysis and Optimization of Baseline Single Aisle Aircraft for Future Electrified Powertrain Flight Demonstration Comparisons," *AIAA AVIATION 2023 Forum*, 2023, p. 3367.

[14] Harish, A., Shi, M., Gladin, J., and Mavris, D., "Advanced 2030 single aisle aircraft modeling for the Electrified Powertrain Flight Demonstration program," *2022 IEEE Transportation Electrification Conference & Expo (ITEC)*, IEEE, 2022, pp. 676–681.

[15] Milios, K., Hall, C., Burrell, A., Brooks, J., Kenny, J., Gladin, J., and Mavris, D., "Modeling and Simulation of a Parallel Hybrid-Electric Propulsion System-Electrified Powertrain Flight Demonstration (EPFD) Program," *2022 IEEE Transportation Electrification Conference & Expo (ITEC)*, IEEE, 2022, pp. 682–687.

[16] Arnson, M., Aljaber, R., and Cinar, G., "Predicting Aircraft Design Parameters using Gaussian Process Regressions on Historical Data," *AIAA SciTech 2025 Forum*, 2025.

[17] Khailany, N., Mokotoff, P. R., and Cinar, G., "Aircraft Geometry and Propulsion Architecture Visualization for the Future Aircraft Sizing Tool (FAST)," *AIAA SciTech Forum*, 2025.

[18] Gray, J. S., Hwang, J. T., Martins, J. R. R. A., Moore, K. T., and Naylor, B. A., "OpenMDAO: An open-source framework for multidisciplinary design, analysis, and optimization," *Structural and Multidisciplinary Optimization*, Vol. 59, No. 4, 2019, pp. 1075–1104. https://doi.org/10.1007/s00158-019-02211-z.

[19] Korn, F., "`mcode.sty` Demo," https://www.overleaf.com/latex/templates/highlighting-matlab-code-in-latex-with-mcode/nhtksndnsmmx.pdf, 2014.

[20] Cinar, G., Garcia, E., and Mavris, D. N., "A framework for electrified propulsion architecture and operation analysis," *Aircraft Engineering and Aerospace Technology*, Vol. 92, No. 5, 2020, pp. 675–684.

[21] Ascher, U. M., and Greif, C., *A first course on numerical methods*, SIAM, 2011.

[22] Cinar, G., "A methodology for dynamic sizing of electric power generation and distribution architectures," Ph.D. thesis, Georgia Institute of Technology, 2018.

[23] De Vries, R., Hoogreef, M. F., and Vos, R., "Range equation for hybrid-electric aircraft with constant power split," *Journal of Aircraft*, Vol. 57, No. 3, 2020, pp. 552–557.

[24] Duffy, K. P., and Jansen, R. H., "Turboelectric and hybrid electric aircraft drive key performance parameters," *2018 AIAA/IEEE Electric Aircraft Technologies Symposium (EATS)*, IEEE, 2018, pp. 1–19.

[25] Anderson, J. D., *Aircraft performance and design*, WCB/McGraw-Hill, Boston, Mass., 1999.

[26] Tremblay, O., and Dessaint, L.-A., "Experimental Validation of a Battery Dynamic Model for EV Applications," *World Electric Vehicle Journal*, Vol. 3, No. 2, 2009, pp. 289–298. https://doi.org/10.3390/wevj3020289.

[27] Mattingly, J. D., Heiser, W. H., Boyer, K. M., Haven, B. A., and Pratt, D. T., *Aircraft Engine Design, Third Edition*, American Institute of Aeronautics and Astronautics, Inc., 2018. https://doi.org/10.2514/4.105173.

[28] Boyce, M. P., *Gas Turbine Engineering Handbook*, 2nd ed., Butterworth-Heinemann, Oxford, England, 2001.

[29] Walsh, P. P., and Fletcher, P., *Gas Turbine Performance*, 2nd ed., Blackwell Science, Philadelphia, PA, 2004.

[30] Saravanamuttoo, H., Rogers, G. F. C., and Cohen, H., *Gas Turbine Theory*, 5th ed., Prentice Hall, Philadelphia, PA, 2001.

[31] Urieli, I., and Ohio University-Athens, "AC 2010-47: Engineering Thermodynamics - A Graphical Approach," 2010.

[32] Hilsenrath, J., Benedict, W. S., Fano, L., Hoge, H. J., masa, J. F., Nuttall, R. L., Touloukian, Y. S., and Woolley, H. W., "Circular of the Bureau of Standards no. 564::tables of thermal properties of gases comprising tables of thermodynamic and transport properties of air, argon, carbon dioxide, carbon monoxide hydrogen, nitrogen, oxygen, and steam," , 1955. https://doi.org/10.6028/NBS.CIRC.564.

[33] Kyle, B. G., *Chemical and process thermodynamics*, Prentice Hall, Old Tappan, NJ, 1999.

[34] Xu, R., Wang, H., Colket, M., and Edwards, T., "Thermochemical properties of Jet Fuels," https://web.stanford.edu/group/haiwanglab/HyChem/approach/Report_Jet_Fuel_Thermochemical_Properties_v6.pdf, Jun. 2015.

[35] European Union Aviation Safety Agency, "ICAO Aircraft Engine Emissions Databank," https://www.easa.europa.eu/en/domains/environment/icao-aircraft-engine-emissions-databank, 2024.

[36] Sun, J., Hoekstra, J. M., and Ellerbroek, J., "OpenAP: An Open-Source Aircraft Performance Model for Air Transportation Studies and Simulations," *Aerospace*, Vol. 7, No. 8, 2020. https://doi.org/10.3390/aerospace7080104.

[37] Meier, N., "Civil Turbojet/Turbofan Specifications," https://jet-engine.net/civtfspec.htm, 2021.

[38] Karnozov, V., "Aviadvigatel Mulls Higher-thrust PD-14s To Replace PS-90A," https://www.ainonline.com/aviation-news/air-transport/2019-08-19/aviadvigatel-mulls-higher-thrust-pd-14s-replace-ps-90a, 2019.

[39] EMBRAER S.A., "Airport planning manual," https://www.embraercommercialaviation.com/wp-content/uploads/2017/02/APM_E175.pdf, 2005.

[40] AIRBUS, "A320neo," https://aircraft.airbus.com/en/aircraft/a320-the-most-successful-aircraft-family-ever/a320neo, 2024.

[41] FSAirlines, "A320neo Specification," https://remote.fsairlines.net/v1/acdetails.php?ac=168100&rvi=19945, 2010.

[42] AIRBUS, "A320 Aircarft characteristics airport and maintenance planning," https://www.airbus.com/sites/g/files/jlcbta136/files/2021-11/Airbus-Commercial-Aircraft-AC-A320.pdf, 2005.

[43] Lockheed Martin Aeronautics Company, "LM-100J," https://www.lockheedmartin.com/content/dam/lockheed-martin/aero/documents/LM-100J/LM-100JBrochure_F2018_Website.pdf, 2018.

[44] Pham, D., Bowles, J. V., Zilliac, G. G., Listgarten, N., Go, S., and Jansen, R. H., "Parametric Modeling and Mission Performance Analysis of a True Parallel Hybrid Turboprop Aircraft for Freighter Operations," *AIAA AVIATION FORUM AND ASCEND 2024*, 2024, p. 3581.

[45] Pham, D. D.-T. V., Recine, C., and Jansen, R. H., "Sizing and Performance Analysis of a MW-Class Electrified Aircraft Propulsion (EAP) System for a Parallel Hybrid Turboprop Concept," *34th Congress of the International Council of the Aeronautical Sciences (ICAS)*, 2024.

[46] Federal Aviation Administration, "Type Certificate Data Sheet No. A1SO," https://drs.faa.gov/browse/excelExternalWindow/6B8971BD3E1EBB4F862584C5006C541A.0001?modalOpened=true, 2019.